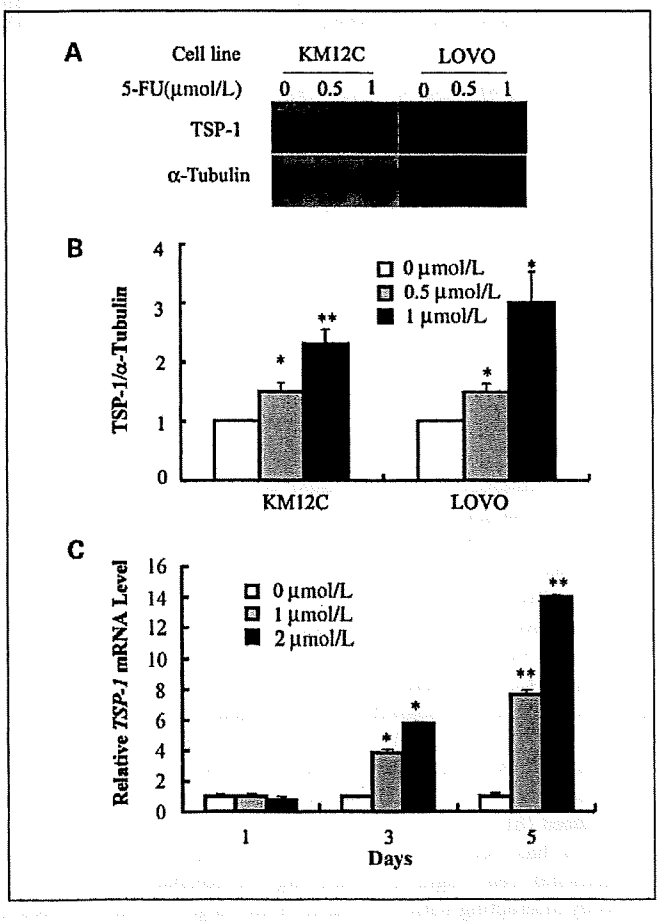

Figure 1. TSP-1 and *TSP-1* mRNA expression induced by 5-FU in human colon cancer cell lines. *A*, effect of 5-FU on TSP-1 protein levels in human colon cancer cell lines. Cells were treated with 5-FU at 0.5 and 1 μmol/L for 4 d. An immunoblot analysis was performed using an antibody against TSP-1. α-Tubulin was used as a loading control. *B*, quantification of relative TSP-1 protein levels. The staining intensities of the bands for TSP-1 and α-tubulin were quantified using NIH image. Protein levels of TSP-1 were normalized to α-tubulin protein levels. Expression levels of TSP-1 are shown relative to that in the untreated cells. *Columns*, average of three independent experiments; *bars*, SD. *, $P < 0.05$, **, $P < 0.01$, significantly different from untreated cells. *C*, effect of 5-FU on *TSP-1* mRNA levels in KM12C cells. Cells were treated with 5-FU at 1 and 2 μmol/L for 1, 3, and 5 d. The relative expression levels of *TSP-1* mRNA in KM12C cells were measured using real-time PCR. The expression of the *GAPDH* gene was used to normalize the values of *TSP-1*. Data are expressed relative to the *TSP-1* mRNA 5-FU–untreated cells at day 1 (considered 1). *Columns*, average of three independent experiments; *bars*, SD. *, $P < 0.05$; **, $P < 0.01$, significantly different from untreated cells on the same day.

according to the manufacturer's instructions. RNA (2 μg) was reverse-transcribed using a ReverTra Ace kit (Toyobo).

Reverse transcription–PCR. The expression levels of *Egr-1* and *TSP-1* were detected using reverse transcription–PCR (RT-PCR). Primer sequences are given in Supplementary Table S1.

Real-time RT-PCR quantification. Expression levels of *TSP-1* and *Egr-1* were determined using real-time PCR (PRISM 7900HT, Applied Biosystems), according to the manufacture's protocol. The sets of primers and TaqMan probes for *glyceraldehyde-3-phosphate dehydrogenase* (*GAPDH*), *TSP-1* and *Egr-1* (4310884E, Hs00170236, and Hs00152928, respectively) were purchased from Applied Biosystems. Human *GAPDH* was used for normalization. Target gene expression was quantified using the comparative cycle threshold method, according to the manufacturer's instructions.

Protein extraction and immunoblotting. KM12C and LOVO cells were plated at a density of 1×10^6 per well in a six-well plate and were treated for 4 d in the absence or presence of 5-FU (0.5 and 1 μmol/L). The cells were harvested and resuspended in lysis buffer [10 mmol/L Tris-HCl (pH 7.5), 25 mmol/L NaCl, 1 mmol/L EDTA, 0.25% Triton X-100, 2 μg/mL aprotinin, 0.5 mmol/L (*p*-amidinophenyl) methanesulfonyl fluoride, 1 mmol/L DTT, and 2 μg/mL leupeptin]. After lysis, the cell debris was removed by centrifugation at 14,000 × *g* for 15 min at 4°C.

The proteins in the whole cell lysate (200 μg) were separated using SDS-PAGE. After electrophoresis, the proteins were transferred to polyvinylidene difluoride membrane and reacted with primary antibodies against TSP-1, Egr-1, phosphorylated HSP27, α-tubulin, and HSP27. After incubation, membranes were washed and incubated with antimouse or antirabbit secondary antibodies (GE Health Science). The membranes were developed using the enhanced chemiluminescence detection system (Amersham Biosciences).

Inhibition of *Egr-1* expression by *Egr-1* small interfering RNA. *Egr-1*–specific small interfering RNA (siRNA) was purchased from Santa Cruz Biotechnology. Transfections (40 nmol/L *Egr-1* siRNA) were accomplished using Lipofectamine 2000 (Invitrogen), according to the manufacturer's protocol. As a control, the cells were treated with an equal amount of *GFP* (eGFP) siRNA (Ambion). After transfection, the cells were exposed to 5-FU (1 and 2 μmol/L) for 5 d and then harvested, and the effect of the siRNA on the expression of *TSP-1* and *Egr-1* was assessed using real-time PCR, RT-PCR, and immunoblotting, as described above.

***TSP-1* promoter-reporter constructs.** Three deletion mutants of pGL3-TSP-1, namely (−1,210/+750), (−267/+750), and (−71/+750), were prepared as described previously (10).

The pGL3–TSP-1 (−2,033/+750) plasmid was constructed as follows. The *TSP-1* promoter, ranging from −2,033 to +750, was amplified using PCR with KOD plus polymerase (Toyobo) from the genomic DNA of KM12C cells using a sense primer (5′-CGGCTAGCCGTCTGCAGAGGCATTCCTACAATCCCTA-CAATCCCTCAGC-3′) and an antisense primer (5′-CCGCTCGAGATCCTG-TAGCAGGAAGCACAAGAGCCGAGG-3′). These primers contained an *Nhe*I or an *Xho*I site at the 5′ end, respectively.

The pGL3–TSP-1 (−2,033/+750 *ΔEgr-1*) plasmid was derived from pGL3–TSP-1 (−2,033/+750) plasmid, deleting the *Sty*I-*Not*I region, including the *Egr-1* binding site.

Transient transfection and dual luciferase reporter assay. KM12C cells were plated at a density of 1×10^5 per well in 24-well plates and pretreated with various concentrations of 5-FU for 3 d before transfection. Transfection and dual-luciferase assay were performed as described previously (11).

Chromatin immunoprecipitation assay. Cells treated with 5-FU, as described above, were fixed with 1% formaldehyde for 10 min at 37°C to cross-link protein to DNA. A chromatin immunoprecipitation (ChIP) assay was carried out using a ChIP assay kit (Upstate Biotechnology), according to the manufacturer's instructions. The soluble DNA fraction was mixed with an anti–Egr-1 antibody or nonimmunized mouse IgG (Santa Cruz Biotechnology), and the precipitated DNA was amplified with primers for the *TSP-1* promoter [5′-AACGAATGGCTCTCTTGGTGT-3′ (sense) and 5′-CTTTCCAGCTAGAAAGTAAG -3′ (antisense)].

Confocal fluorescence microscopy. KM12C cells (7.5×10^4) were cultured in the medium with or without 2 μmol/L 5-FU for 5 d on coverslips, fixed with 3% formaldehyde in PBS for 10 min at room temperature, and permeabilized with 100% methanol for 10 min. Cells were incubated with an antibody against Egr-1 at 4°C overnight. After washing thrice in PBS, the cells were incubated with 200-fold diluted Alexa Fluor 546–labeled antirabbit IgG (Invitrogen). Nuclei were stained by incubating cells with 6 μmol/L 4′,6-diamidino-2-phenylindole (DAPI). The cells were observed using confocal flurorescence microscopy (FV500, Olympus Corporation).

Statistical analysis. Statistical comparisons were performed using the Student's *t* test. Quantitative data were expressed as the means ± SD. $P < 0.05$ was considered significant.

Results

Expression of TSP-1 protein induced by 5-FU in human colon cancer cell lines. Our recent results have shown that the

5-FU–based drug, S-1, at sub-MTD concentration has antiangiogenic function through up-regulation of TSP-1 in colorectal cancer xenografts (5). To investigate possible mechanisms underlying the specificity of this effect, human colon cancer cells were treated with 5-FU at concentrations near or below IC_{50} for 4 days (Supplementary Fig. S1). The expression of TSP-1 in two human colon cancer cell lines was then determined by immunoblot analysis using an antibody against TSP-1. When KM12C and LOVO cells were treated with 5-FU at 1 μmol/L, the expression levels of TSP-1 were 3-fold and 2-fold increased, compared with counterpart untreated cells, respectively (Fig. 1*A* and *B*). Meanwhile, treatment of the cells with 10 μmol/L 5-FU for 1 day also increased the expression of TSP-1 protein in KM12C cells (data not shown). In this study, we focused on the molecular basis for the induction of TSP-1 by low-dose 5-FU. Because the TSP-1 protein level in KM12C cells treated with 5-FU was considerably higher than that in 5-FU–treated LOVO cells, we used KM12C cells for further study.

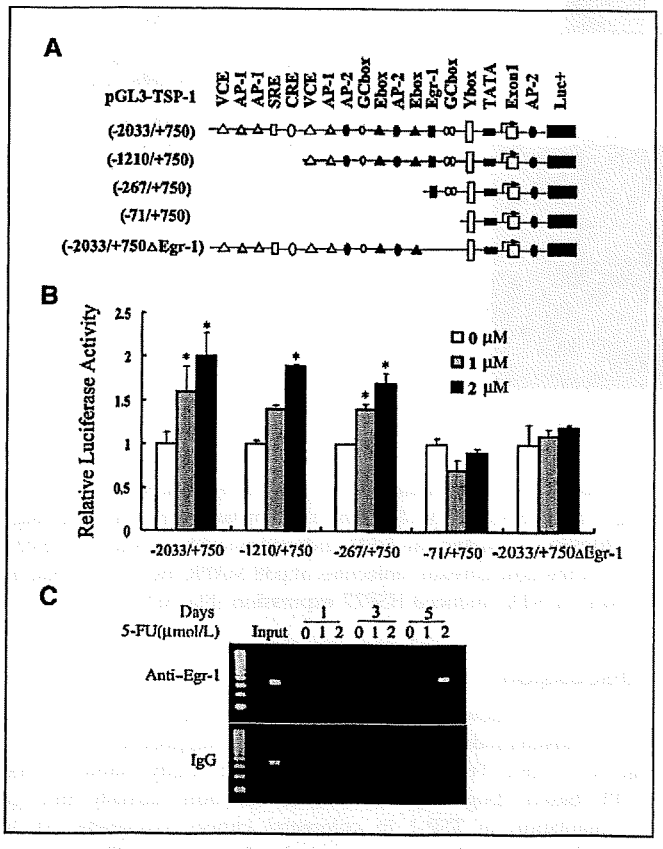

Figure 2. Effect of 5-FU on *TSP-1* promoter activity. *A*, schematic representation of a series of *TSP-1* promoter deletion constructs. The Egr-1–binding site is indicated by the closed square. *B*, KM12C cells were pretreated for 3 d with 5-FU, and these constructs were transiently transfected to the cells using Lipofectamine. The cells were further incubated with or without 2 μmol/L 5-FU for 48 h and harvested, and their luciferase activities were determined. The luciferase activities were corrected for differences in transfection efficiency among wells, as estimated using the *Renilla* luciferase activities. *Columns*, representative of triplicate independent experiments; *bars*, SD. *, $P < 0.05$, significantly different from untreated cells transfected with the same construct. *C*, binding of Egr-1 to *TSP-1* promotor in KM12C cells. KM12C cells were treated with 5-FU at 1 and 2 μmol/L for 1, 3, and 5 d. The cells were fixed with formaldehyde to form a DNA-protein complex and were subjected to a ChIP assay, as described in the Materials and Methods. PCR for the core promoter region of the *TSP-1* gene was performed using DNA extracted from the DNA-protein complex immunoprecipitated using an anti–Egr-1 antibody or nonimmune IgG.

Effect of 5-FU on the expression of the *TSP-1* gene in KM12C cells. The levels of *TSP-1* mRNA in KM12C cells incubated in the absence or presence of 5-FU were determined using real-time RT-PCR. Treatment of the KM12C cells with 5-FU at 1 and 2 μmol/L for 1, 3, and 5 days increased the *TSP-1* mRNA levels in a dose-dependent and time-dependent manner compared with those in untreated cells (Fig. 1*C*). Furthermore, the expression level of *TSP-1* mRNA in human umbilical vein endothelial cells treated with 5-FU was ~2-fold higher than in the untreated cells (data not shown). These data suggested that 5-FU enhanced TSP-1 protein expression in both cancer and endothelial cells by activating transcription of *TSP-1* gene.

Identification of the transcriptional regulatory element necessary for transcriptional activation of the *TSP-1* gene by 5-FU. To investigate which transcriptional regulatory elements in the *TSP-1* promoter contribute to the transcriptional activation of the *TSP-1* gene by 5-FU, we made wild-type and various deletion constructs of the *TSP-1* promoter (Fig. 2*A*). The 5′-flanking region up to −2,033 from the transcription initiation site contained several putative binding sites for known transcription factors, including an Egr-1 site and Sp-1 sites (GC boxes; Fig. 2*A*). The longest construct (−2,033/+750) showed the highest promoter activity among the constructs in the cells treated with 5-FU, and the activity was considerably decreased when the constructs lacked the region including both the Egr-1 and Sp-1 binding sites (Fig. 2*B*). These findings suggested that Egr-1 or Sp-1 transcription factors might enhance the expression of the *TSP-1* gene.

***TSP-1* promoter and its *in vivo* Egr-1 recruitment.** DNA-damaging agents can up-regulate the expression of the tumor suppressor gene *Egr-1* in both normal and cancer cells (12), whereas Sp-1 plays a role in the EGF-induced activation of the *TSP-1* gene (10). We thus focused our study on Egr-1. To confirm the recruitment of Egr-1 to the *TSP-1* promoter *in vivo*, a ChIP assay was performed (Fig. 2*C*). The Egr-1 recruitment was dose-dependently and time-dependently enhanced by 5-FU in KM12C cells. This enhancement was hardly detected when nonimmune IgG was used (Fig. 2*C*, *bottom*). These results indicated the enhanced binding of Egr-1 to the *TSP-1* promoter in cells treated with 5-FU.

Effect of 5-FU on Egr-1 expression in KM12C cells. The expression of *Egr-1* mRNA was also verified using RT-PCR and real-time PCR (Fig. 3). It was dose-dependently and time-dependently increased by 5-FU (Fig. 3*A* and *B*). To identify the subcellular localization of Egr-1 induced by 5-FU, Egr-1 was observed using confocal fluorescence microscopy. Egr-1 was mainly localized in the nuclei of KM12C cells treated with 5-FU but was not detected in the control cells (Fig. 3*C*).

Effect of *Egr-1* knockdown on the induction of *TSP-1* by 5-FU. To confirm that Egr-1 is involved in the enhanced expression of TSP-1 by 5-FU, *Egr-1* siRNAs were used to knockdown the expression of *Egr-1*. The induction of *Egr-1* mRNA and protein expression by 5-FU was considerably suppressed by *Egr-1* siRNA, but not by *GFP* siRNA. *Egr-1* knockdown resulted in the decreased expression of *TSP-1* mRNA and protein (Fig. 4*A–D*). These results show that Egr-1 is required for the 5-FU–mediated induction of TSP-1.

To examine whether Egr-1 is required for the 5-FU–mediated induction of TSP-1 in other tumor cells, we determined the expression levels of Egr-1 and TSP-1 in MCF7 cells. When MCF7 cells were treated with 1 and 2 μmol/L 5-FU at concentrations near IC_{50} (Supplementary Fig. S2*A*), the expressions of Egr-1 and

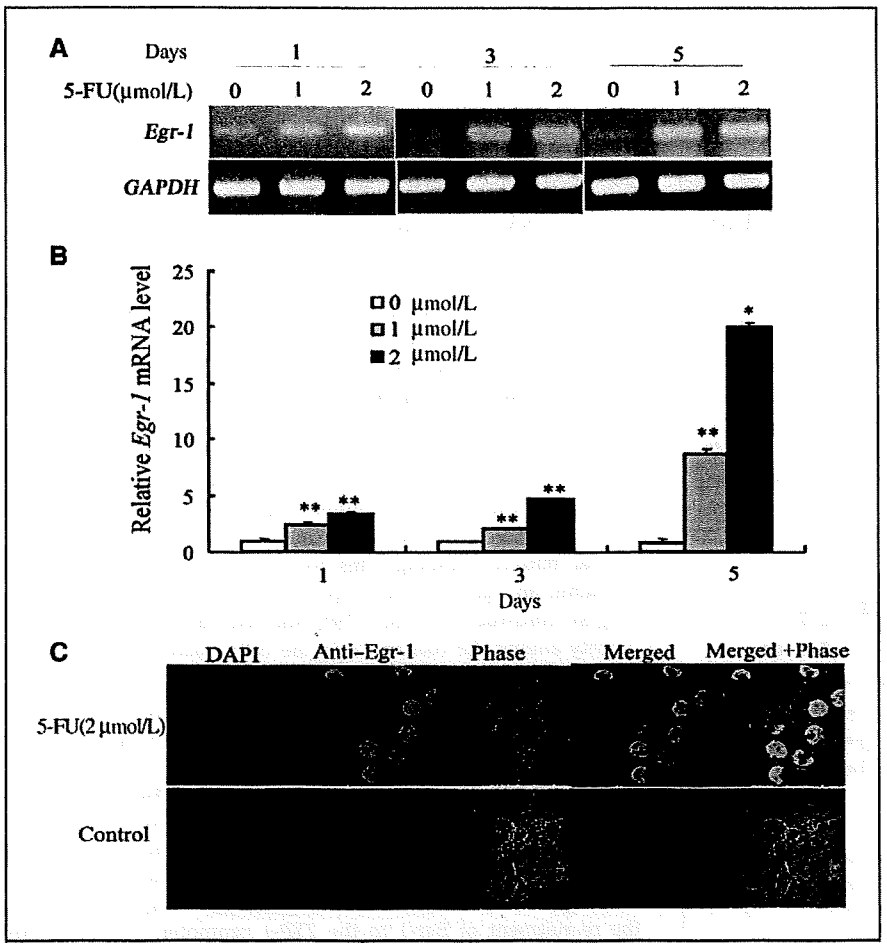

Figure 3. Effect of 5-FU on Egr-1 expression in KM12C cells. *A* and *B*, cells were treated with 5-FU at 1 and 2 μmol/L for 1, 3, and 5 d, and the *Egr-1* mRNA was analyzed using RT-PCR. *A*, semiquantitative RT-PCRs performed with primers specific for the indicated genes. *B*, relative expression levels of *Egr-1* mRNA in KM12C cells were measured using real-time PCR. The expression of the *GAPDH* gene was used to normalize the values of *Egr-1*. Data are expressed relative to the *Egr-1* mRNA level in untreated cells at day 1 (considered 1). *Columns*, representative of triplicate independent experiments; bars, SD. *, $P < 0.05$; **, $P < 0.01$, significantly different from untreated cells. *C*, nuclear localization of Egr-1 protein induced by 5-FU in KM12C cells. The intracellular localization of Egr-1 was analyzed using confocal fluorescence microscopy. The cells were treated with 2 μmol/L 5-FU for 5 d and stained with DAPI (*blue*) and an anti–Egr-1 antibody (*green*). *Top*, KM12C cells treated with 2 μmol/L 5-FU; *bottom*, untreated cells.

TSP-1 were also increased compared with those of untreated cells (Supplementary Fig. S2*B–D*). TSP-1 protein levels in the 5-FU–treated MCF7 cells were suppressed when Egr-1 was down-regulated by *Egr-1* siRNA (data not shown). These results suggest that our findings are not limited to KM12C cells.

Effect of 5-FU on the activation of the p38 MAPK pathway. Several studies have indicated the activation of one or more members of the MAPK family of intracellular signaling kinases by cytotoxic agents (13). Among them, p38 often transmits the signal generated by diverse stimuli (14). The p38 MAPK inhibitor SB203580 attenuated the TSP-1 up-regulation induced by trastuzumab and transforming growth factor-β1 (TGF-β1; refs. 10, 15). We thus focused our study on p38 MAPK. To examine whether 5-FU is involved in the activation of the MAPK pathways, the effect of 5-FU on the phosphorylation of proteins involved in p38 MAPK pathways was studied. The treatment of KM12C cells with 1 and 2 μmol/L 5-FU for 5 days increased the phosphorylation of p38, whereas the expression level of p38 remained unchanged (Fig. 5*A*). This indicated that the p38 MAPK pathway is activated by 5-FU.

Effect of p38 MAPK inhibitor on 5-FU–induced Egr-1 and *TSP-1* expression. To confirm that the activation of p38 MAPK contributes to 5-FU–induced Egr-1 and TSP-1 expression, we examined the effect of a p38 MAPK inhibitor on the expression of Egr-1 and TSP-1. As shown in Fig. 5, the p38 MAPK inhibitor SB203580 remarkably suppressed the expression of *Egr-1*, *TSP-1* mRNA, and Egr-1 (Fig. 5*B–D*). The p38 MAPK signaling pathway might play an important role in the 5-FU–induced expression of Egr-1 and *TSP-1* in KM12C cells. In accordance with these findings, SB203580 attenuated the 5-FU–induced phosphorylation of HSP27, one of the downstream molecules of p38 MAPK. However, it had no effect on 5-FU–induced HSP27 expression (Fig. 5*D*).

Discussion

Previous studies indicated that TSP-1 induced by low-dose cyclophosphamide is implicated in the suppression of tumor growth (16). Furthermore, our recent study showed that 5-FU–based drugs have antitumor function partially through up-regulation of TSP-1 in colorectal cancer xenografts (5). In accordance with these results, we also found that 5-FU enhanced the expression of TSP-1 in human colon cancer (KM12C and LOVO cells) and breast cancer MCF7 cells (Fig. 1 and Supplementary Fig. S2*B* and *D*). The expression level of *TSP-1* mRNA in human umbilical vascular endothelial cell was also increased by 5-FU (data not shown). Various extracellular stimuli and compounds altered *TSP-1* gene expression (17). It is generally accepted that TSP-1 expression levels are tightly regulated at the transcriptional level. Donoviel and colleagues (18) identified the *TSP-1* promoter region and found that the 5′-flanking region between −234 and +750 was important for the basal transcriptional activity (19). The promoter region of mouse *TSP-1* contains one Egr-1 binding site, and *TSP-1* transcription is enhanced by

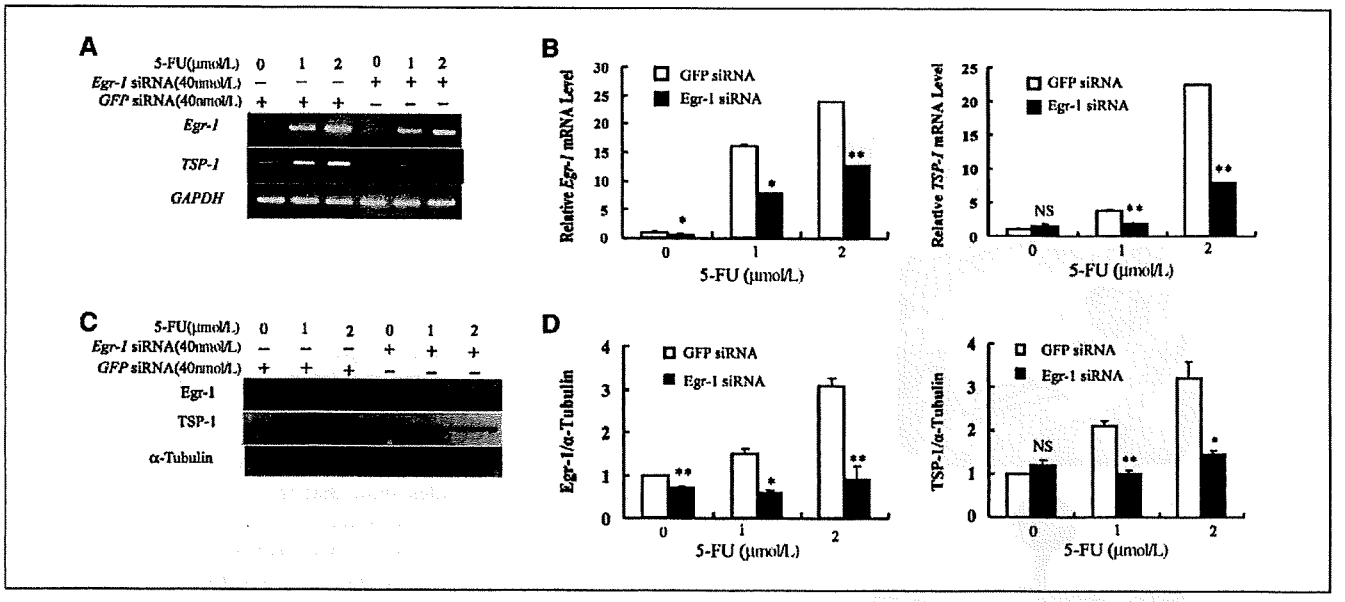

Figure 4. Effect of *Egr-1* knockdown on the induction of *TSP-1* in KM12C cells treated with 5-FU. KM12C cells were transfected with 40 nmol/L *Egr-1* siRNA for 6 h and then subjected to 5-FU at 2 μmol/L for 5 d. *A*, semiquantitative RT-PCRs performed with primers specific for the indicated genes. *B*, the levels of *Egr-1* (*left*) and *TSP-1* (*right*) mRNA were measured using real-time RT-PCR. The *GAPDH* gene was used to normalize the values of *TSP-1* and *Egr-1* mRNAs. Data are expressed relative to the *Egr-1* or *TSP-1* mRNA level in *GFP* siRNA-transfected and 5-FU–untreated cells. *Columns*, an average of three independent experiments; *bars*, SD. *, $P < 0.05$; **, $P < 0.01$, significantly different from *GFP* siRNA-transfected cells treated with the same concentrations of 5-FU. *C*, the expression level of Egr-1 and TSP-1 in 5-FU–treated KM12C cells transfected with *GFP* or *Egr-1* siRNA was analyzed. The cell lysates were subjected to SDS-PAGE, and the expressions of Egr-1 and TSP-1 were detected using immunoblotting with the antibodies indicated in Materials and Methods. *D*, Egr-1 (*left*) and TSP-1 (*right*) protein levels were determined as described in Fig. 1*B*. Data are expressed relative to the levels of Egr-1 or TSP-1 in *GFP* siRNA-transfected and 5-FU–untreated cells. *Columns*, an average of three independent experiments; *bars*, SD. *, $P < 0.05$; **, $P < 0.01$, significantly different from *GFP* siRNA-transfected cells untreated with 5-FU.

Egr-1 (20). In human hepatic HuH-7 cells, the *TSP-1* promoter region between −267 and −71 contained two GC boxes to which Sp-1 bound. These boxes were found to be responsible for the promoter activity enhanced by EGF (10). Consistent with these studies, we also showed that *TSP-1* promoter region (−267/−71) is needed for the augmentation *TSP-1* promoter activity by 5-FU, and the deletion of the region in which the Egr-1 and SP-1 binding sites reside almost completely blocked the *TSP-1*

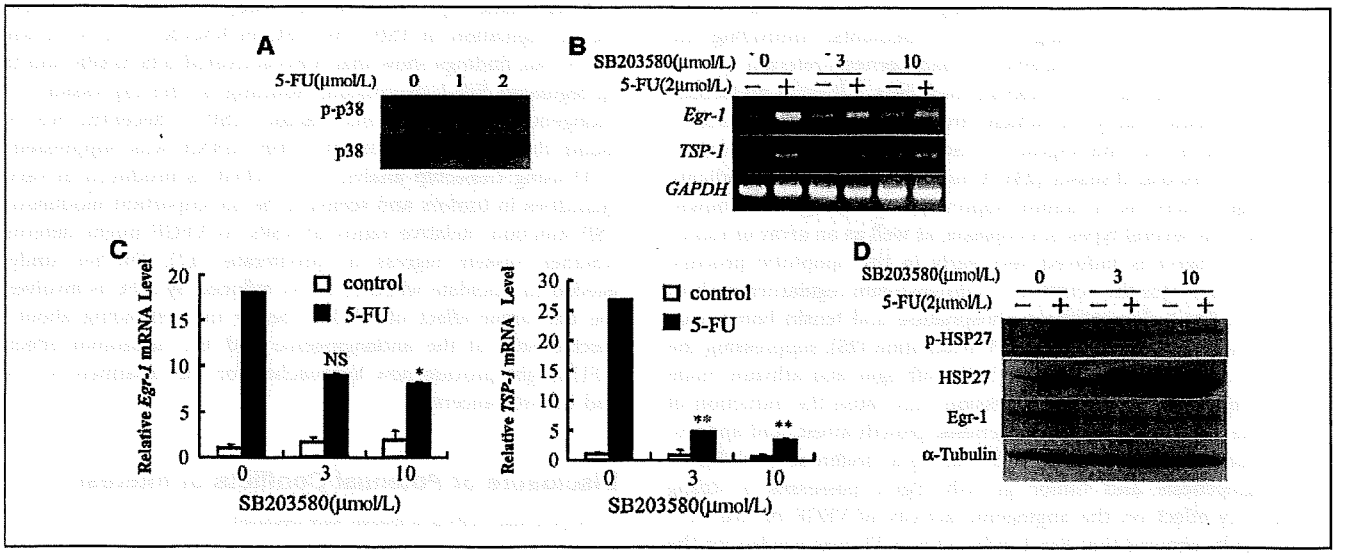

Figure 5. Activation of p38 MAPK pathway by 5-FU and the effect of the activated p38 MAPK pathway on the 5-FU–induced expression of *TSP-1* mRNA levels and Egr-1 expression in KM12C cells. *A*, KM12C cells were exposed to 1 or 2 μmol/L of 5-FU for 5 d, and an immunoblot analysis was performed using an antibody against phosphorylated p38 kinase. The blot was reprobed with an antibody against p38. KM12C cells were treated as described above, and 5-FU–induced *Egr-1* and *TSP-1* mRNA levels were measured using semiquantitative RT-PCR and real-time RT-PCR. *B*, semiquantitative RT-PCRs performed with primers specific for the indicated genes. *C*, relative expression levels of *Egr-1* (*left*) and *TSP-1* (*right*) mRNAs in KM12C cells were measured using real-time RT-PCR. The expression of the *GAPDH* gene was used to normalize the values of *Egr-1* and *TSP-1*. Data are expressed relative to the *Egr-1* or *TSP-1* mRNA in the untreated cells. *Columns*, an average of three independent experiments; *bars*, SD. *, $P < 0.05$; **, $P < 0.01$, significantly different compared with the cells treated with 2 μmol/L 5-FU alone. *D*, KM12C cells were exposed to 2 μmol/L 5-FU with or without MAPK inhibitor for 5 d, and an immunoblot analysis was performed using the indicated antibodies. α-Tubulin was used as an internal control.

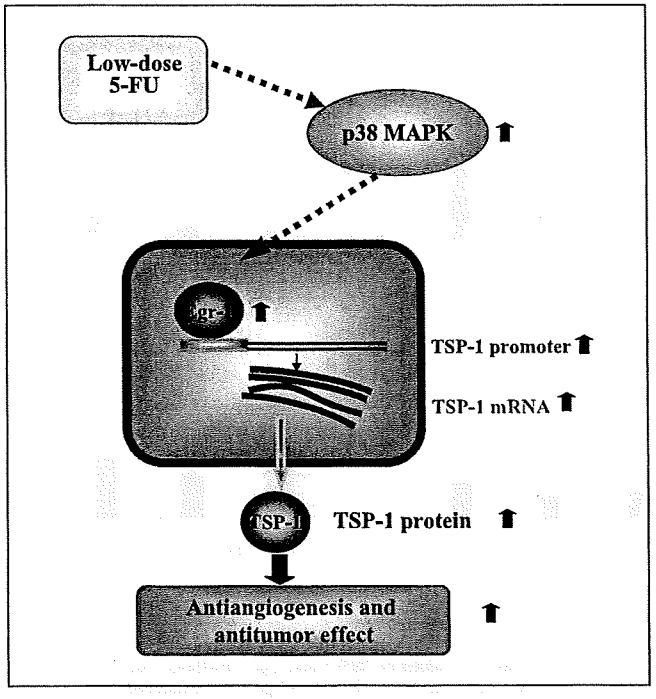

Figure 6. Schematic pathway for 5-FU–induced TSP-1 expression in KM12C human colon cancer cells. In this model, 5-FU causes the activation of the p38 MAP kinase pathway, leading to the increased expression of Egr-1. Egr-1 binds to the promoter of *TSP-1* and enhances the transcription of the *TSP-1* gene and subsequently the expression of Egr-1.

promoter activity (Fig. 2*B*). Furthermore, the increased binding of Egr-1 to the *TSP-1* promoter in cells treated with 5-FU was also observed (Fig. 2*C*).

Egr-1 is a Cys2-His2–type zinc-finger transcription factor and binds to GC-rich, *cis*-acting promoter elements, controlling the expression of a wide variety of pathogenesis-relevant genes, encoding growth factors, cytokines, receptors, adhesion molecules, and proteases, many of which are involved in angiogenesis, tumorigenesis (21), the response to ischemia (22), and the progress of several vascular diseases (23). A number of reports also indicate that *Egr-1* acts as a tumor suppressor gene. Egr-1 is down-regulated in several types of neoplasia, as well as an array of tumor cell lines. Egr-1 is induced very early in the apoptotic process, where it mediates the activation of downstream regulators, such as p53 (24). Egr-1 also activates phosphatase and tensin homologue tumor suppressor gene during UV irradiation (25), suppressing the growth of transformed cells in both soft agar and athymic nude mice (26). Sustained Egr-1 expression may cause the induction of multiple pathways of antiangiogenesis, growth arrest, and apoptosis induction in proliferating cells leading to preferential inhibition of angiogenesis and tumor growth. Egr-1 possesses a strong inhibitory effect on the angiogenic activity of VEGF *in vivo* (27). Our results showed that Egr-1 induced by 5-FU was needed for the increased expression of TSP-1 in KM12C cells treated with 5-FU (Figs. 3 and 4).

MAPK pathways have been implicated in the response to chemotherapeutic drugs (28). c-Jun amino-terminal kinase and p38 kinase are important for controlling cell growth and apoptosis in response to chemical stress, radiation, and growth factors (29). Our results showed that 5-FU activated p38 MAPK (Fig. 5*A*). Activated p38 MAPK phosphorylates MAPKAP kinase 2, which in turn phosphorylates HSP27 (30). SB203580 attenuated the 5-FU–enhanced phosphorylation of HSP27, indicating that SB203580 effectively inhibited the activation of p38 pathway in 5-FU–treated KM12C cells. SB203580 suppressed the expression of both *Egr-1* and *TSP-1* mRNAs, suggesting that the activation of the p38 MAPK pathway by 5-FU is responsible for the induction of Egr-1 and TSP-1 (Fig. 5*B–D*). Trastuzumab also stimulated sustained p38 activation, and SB203580 attenuated the TSP-1 up-regulation induced by trastuzumab (15). SB203580 partially inhibited TGF-β1–induced TSP-1 expression (10). These findings suggest that the activation of p38 MAPK plays an important role in the induction of TSP-1 by some anticancer agents and growth factors. Further study is needed to determine the detailed mechanisms underlying the regulation of the p38 MAPK pathway by 5-FU.

Several transcription factors are regulated by p38 MAPK, and this kinase is involved in the control of the expression of various genes. *In vitro* studies show that the transcription factor ATF2 is phosphorylated and activated by p38 MAPK. In addition, p38 MAPK activates the Elk-1, CHOP, MEF2C, and SAP-1 transcription factors (31). Our finding that 5-FU activated p38 MAPK and then increased the expression of Egr-1 may be useful for elucidating the molecular basis for the chemopreventive and antitumor effects of 5-FU and its prodrugs.

HSP27 is a molecular chaperone that is constitutively expressed in several mammalian cells, particularly during pathologic conditions. This protein protects cells against toxicity mediated by aberrantly folded proteins or oxidative inflammatory conditions. In addition, this protein has antiapoptotic properties and is tumorigenic when expressed in cancer cells (32). Some anticancer agents, particularly cisplatin (33), vincristine, and colchicines (34), also enhanced HSP27 expression. It is as yet unknown whether the induced HSP27 affects the antitumor activity of these anticancer agents.

A schematic representation of a proposed molecular basis for the up-regulation of TSP-1 by 5-FU in KM12C cells is shown in Fig. 6. Our findings show that 5-FU activated p38 MAPK and then up-regulated Egr-1 expression, resulting in the expression of an endogeneous antiangiogenic factor, TSP-1. Recently, we have found that the expression of *VEGF* mRNA was suppressed by 5-FU using Genechip analysis (11). VEGF is produced in varying quantities in tumors and seems to be an important modulator of TSP function. Relative ratios of TSPs to VEGF might determine whether vessels regress or proliferate (17). Further study is needed to elucidate whether TSP-1 induced by 5-FU is involved in the antitumor effect of 5-FU. A better understanding about the mechanisms of the antiangiogenic and the antitumor effect of 5-FU might provide new approaches for the treatment of colon and breast cancers.

Disclosure of Potential Conflicts of Interest

No potential conflicts of interest were disclosed.

Acknowledgments

Received 12/7/2007; revised 6/17/2008; accepted 6/27/2008.

Grant support: Ministry of Education, Culture, Sports, Science and Technology grant-in-aid and Kobayashi Institute for Innovative Cancer Chemotherapy grants.

The costs of publication of this article were defrayed in part by the payment of page charges. This article must therefore be hereby marked *advertisement* in accordance with 18 U.S.C. Section 1734 solely to indicate this fact.

We thank Hiromi Mitsuo for her valuable secretarial assistance.

References

1. Schipper DL, Wagener DJ. Chemotherapy of gastric cancer. Anticancer Drugs 1996;7:137–49.
2. Tanaka F. UFT (Tegafur and Uracil) as postoperative adjuvant chemotherapy for solid tumors (Carcinoma of the lung, stomach, colon/rectum, and breast): clinical evidence, mechanism of action, and future direction. Surg Today 2007;37:923–43.
3. Ho DH, Pazdur R, Covington WP, et al. Comparison of 5-fluorouracil pharma-cokinetics in patients receiving continuous 5-fluorouraci infusion and oral uracil plus 1-5(2-tertahydrofuryl)-5-fluorouracil. Clin Cancer Res 1998;4:2085–8.
4. Munoz R, Man S, Shaked Y, et al. Advanced metastatic breast cancer using combination oral UFT-cyclophosphamide metronomic chemotherapy. Cancer Res 2006; 66:3386–91.
5. Ooyama A, Oka T, Zhao HY, et al. Anti-angiogenic effect of 5-Fluorouracil-based drugs against human colon cancer xenografts. Cancer Lett 2008;267:26–36.
6. Malet-Martino M, Martino R. Clinical studies of three oral prodrugs of 5-fluorouracil. Oncologist 2002;7:288–323.
7. Ren B, Yee KO, Lawler J, Khosravi-Far R. Regulation of tumor angiogenesis by thrombospondin-1. Biochim Biophys Acta 2006;1765:178–88.
8. Shaked Y, Bertolini F, Man S, et al. Genetic heterogeneity of the vasculogenic phenotype parallels angiogenesis; implications for cellular surrogate marker analysis of antiangiogenesis. Cancer Cell 2005;7:101–11.
9. Munoz R, Shaked Y, Bertolini F, et al. Anti-angiogenic treatment of breast cancer using metronomic low-dose chemotherapy. Breast 2005;14:466–79.
10. Okamoto M, Ono M, Uchiumi T, et al. Up-regulation of thrombospondin-1gene by epidermal growth factor and transforming growth factor β in human cancer cells-transcriptional activation and messenger RNA stabilization. Biochim Biophys Acta 2002;1574:24–34.
11. Zhao HY, Ooyama A, Yamamoto M, et al. Down regulation of *c-Myc* and induction of an angiogenesis inhibitor, thrombospondin-1, by 5-FU in human colon cancer KM12C cells. Cancer Lett. In press. 2008.
12. Quinones A, Dobberstein KU, Rainov NG. The egr-1 gene is induced by DNA-damaging agents and non-genotoxic drugs in both normal and neoplastic human cells. Life Sci 2003;2:297–5.
13. Srivastava RK, Mi QS, Hardwick JM, Longo DL. Deletion of the loop region of Bcl-2 completely blocks paclitaxel-induced apoptosis. Proc Natl Acad Sci U S A 1999;96:3775–80.
14. Hazzalin CA, Cuenda A, Cano E, et al. Effects of the inhibition of p38/RK MAP kinase on induction of five fos and jun genes by diverse stimuli. Oncogene 1997;15: 2321–31.
15. Wen XF, Yang G, Mao W, et al. HER2 signaling modulates the equilibrium between pro- and antiangiogenic factors via distinct pathways: implications for HER2-targeted antibody therapy. Oncogene 2006;25: 6986–96.
16. Bocci G, Francia G, Man S, Lawler J, Kerbel RS. Thrombospondin 1, a mediator of the antiangiogenic effects of low-dose metronomic chemotherapy. Proc Natl Acad Sci U S A 2003;100:12917–22.
17. Armstrong LC, Bornstein P. Thrombospondins 1 and 2 function as inhibitors of angiogenesis. Matrix Biol 2003;22:63–71.
18. Donoviel DB, Framson P, Eldridge CF, et al. Structural analysis and expression of the human thrombospondin gene promoter. J Biol Chem 1988;263:18590–93.
19. Laherty CD, Gierman TM, Dixit VM. Characterization of the promoter region of the human thrombospondin gene. DNA sequences within the first intron increase transcription. J Biol Chem 1989;264:11222–7.
20. Shingu T, Bornstein P. Overlapping Egr-1 and Sp1 sites function in the regulation of transcription of the mouse thrombospondin 1 gene. J Biol Chem 1994;269: 32551–7.
21. Fahmy RG, Dass CR, Sun LQ, Chesterman CN, Khachigian LM. Transcription factor Egr-1 supports FGF-dependent angiogenesis during neovascularization and tumor growth. Nat Med 2003;9:1026–32.
22. Yan SF, Fujita T, Lu J, et al. Egr-1, a master switch coordinating upregulation of divergent gene families underlying ischemic stress. Nat Med 2000;6:1355–61.
23. Silverman ES, Collins T. Pathways of Egr-1-mediated gene transcription in vascular biology. Am J Pathol 1999; 154:665–70.
24. Pignatelli M, Luna-Medina R, Perez-Rendon A, Santos A, Perez-Castillo A. The transcription factor early growth response factor-1 (EGR-1) promotes apoptosis of neuroblastoma cells. Biochem J 2003;373: 739–46.
25. Virolle T, Adamson ED, Baron V, et al. The Egr-1 transcription factor directly activates PTEN during irradiation-induced signalling. Nat Cell Biol 2001;3: 1124–8.
26. Huang RP, Darland T, Okamura D, Mercola D, Adamson ED. Suppression of v-sis-dependent transformation by the transcription factor, Egr-1. Oncogene 1994;9:1367–77.
27. Lucerna M, Pomyje J, Mechtcheriakova D, et al. Sustained expression of early growth response protein-1 blocks angiogenesis and tumor growth. Cancer Res 2006;66:6708–13.
28. Makin G, Dive C. Modulating sensitivity to drug-induced apoptosis: the future for chemotherapy. Breast Cancer Res 2001;3:150–3.
29. Johnson GL, Lapadat R. Mitogen-activated protein kinase pathways mediated by ERK, JNK, p38 protein kinases. Science 2002;298:1911–2.
30. Rouse J, Cohen P, Trigon S, et al. A novel kinase cascade triggered by stress and heat shock that stimulates MAPKAP kinase-2 and phosphorylation of the small heat shock proteins. Cell 1994;78:1027–37.
31. Rolli M, Kotlyarov A, Sakamoto KM, et al. Stress-induced stimulation of early growth response gene-1 by p38/stress-activated protein kinase 2 is mediated by a cAMP-responsive promoter element in a MAPKAP kinase 2-independent manner. J Biol Chem 1999;274: 9559–64.
32. Arrigo AP, Simon S, Gibert B, et al. Hsp27 (HspB1) and αB-crystallin (HspB5) as therapeutic targets. FEBS Lett 2007;581:3665–74.
33. Oesterreich S, Schunck H, Benndorf R, Bielka H. Cisplatin induces the small heat shock protein hsp25 and thermotolerance in Ehrlich ascites tumor cells. Biochem Biophys Res Commun 1991;180:243–8.
34. Kato K, Ito H, Inaguma Y, et al. Synthesis and accumulation of αB crystallin in C6 glioma cells is induced by agents that promote the disassembly of microtubules. J Biol Chem 1996;271:26989–94.

Inhibition of bone and muscle metastases of lung cancer cells by a decrease in the number of monocytes/macrophages

Koji Hiraoka,[1,2,7] Michihisa Zenmyo,[1,2] Kousuke Watari,[3] Haruo Iguchi,[4] Abbas Fotovati,[2] Yusuke N. Kimura,[2] Fumihito Hosoi,[2] Takanori Shoda,[1,2] Kensei Nagata,[1,2] Hiroyuki Osada,[5] Mayumi Ono[3,6] and Michihiko Kuwano[2,6]

[1]Department of Orthopedic Surgery and [2]Research Center of Innovative Cancer Therapy, Kurume University School of Medicine, Kurume 830-0011; [3]Department of Pharmaceutical Oncology, Graduate School of Pharmaceutical Sciences, Kyushu University, Fukuoka 812-8582; [4]Clinical Research Institute, Shikoku Cancer Center, Matsuyama 791-0280; [5]Antibiotics Laboratory, Discovery Research Institute, RIKEN, Saitama 351-0198; [6]Innovative Center for Medical Redox Navigation, Kyushu University, Fukuoka 812-8582, Japan

(Received December 25, 2007/Revised April 20, 2008/Accepted April 29, 2008/Online publication July 29, 2008)

Attention has recently focused on the critical role of inflammatory responses in the tumor stroma that provide favorable conditions for cancer-cell growth and invasion/metastasis. In particular, macrophages recruited into the tumor stroma and activated, known as tumor-associated macrophages, are suggested to promote tumorigenesis. In this study, we examined the effect of a decrease in the number of monocytes/macrophages in peripheral blood and the tumor stroma on the development of bone and muscle metastases by lung cancer cells. Treatment with clodronate encapsulated by liposomes (Cl_2MDP-LIP) has been developed for the depletion of monocytes/macrophages in an animal model. Subcutaneous administration of Cl_2MDP-LIP markedly reduced the number of monocytes in peripheral blood, resulting in efficient suppression of both bone metastasis and muscle metastasis when lung cancer HARA-B cells were injected into the left cardiac ventricle of mice. Treatment with Cl_2MDP-LIP significantly reduced the number of macrophages in tumors and the number of osteoclasts in bone marrow, as well as peripheral monocytes in mice harboring lung cancer cells. In contrast, treatment with an osteoclast-targeting antibiotic, reveromycin A, inhibited bone metastasis by lung cancer cells, but not muscle metastasis. The survival of human macrophages in culture was found to be specifically blocked by Cl_2MDP-LIP, but not by reveromycin A. Cl_2MDP-LIP thus exerted antimetastatic effects in both bone and muscle whereas reveromycin A did so only in bone. Liposome-encapsulated bisphosphonate may modulate metastasis through decreasing the number of monocytes/macrophages in both peripheral blood and the tumor stroma, suggesting that tumor-associated macrophages might be suitable targets for antimetastatic therapy. (*Cancer Sci* 2008; 99: 1595–1602)

Metastases of several malignant cancers including those of the breast, lung, prostate, and kidney have high affinity for bone. Bone metastasis is often accompanied by serious complications such as pathological fractures, bone pain, spinal cord compression, and hypercalcemia. Organ metastasis, including that affecting bone, is a multistep process mediated through mutual interaction between cancer cells and the host microenvironment. In bone metastasis, cancer cells reach the bone via hematogenous spread, followed by osteoclastic bone resorption, and finally proliferate in the bone matrix.[1,2] Moreover, osteoclast-stimulating cytokines such as PTHrP have been shown to promote bone metastasis.[3]

Inflammatory responses in the tumor stroma play an important role by providing favorable conditions for cancer cell growth, invasion/metastasis, and angiogenesis as well as malignant progression.[4–6] In particular, monocytes/macrophages are recruited into the tumor stroma, and activated macrophages known as TAMs produce potent angiogenic factors, as well as inflammatory cytokines, growth factors, and proteases, resulting in a promotion of angiogenesis and invasion/metastasis.[7–9] Infiltrating TAMs are often closely associated with poor prognosis and tumor angiogenesis in patients with various tumor types.[9–11] A preparation of Cl_2MDP-LIP has been reported to markedly inhibit angiogenesis in corneas in response to inflammatory cytokines through depletion of macrophages.[12] A recent study has demonstrated that administration of clodronate-liposomes depleted TAMs in mouse models resulting in significant inhibition of tumor growth and tumor angiogenesis, whereas free clodronate alone did not.[13] Clodronate-liposomes were also found to inhibit both tumor growth and tumor angiogenesis by lung cancer cells in a xenograft model when stimulated by inflammatory stimuli.[14] Angiogenesis in a tumor microenvironment in bone marrow also played a critical role in the induction of an angiogenic response and invasion/metastasis by cancer cells.[15] Furthermore, monocyte/macrophage precursor cells entered the osteoclastic lineage and expressed the osteoclastic marker TRAP under the influence of the RANK/RNAKL signaling pathway.[16] Tumor burden at bone metastatic sites was markedly decreased in preclinical models on treatment with inhibitors of the RANK/RANKL pathway and neutralizing antibodies against PTHrP as well as bisphosphonate, suggesting a central role for osteoclasts in bone metastasis.[17–19] Together, one can expect a decrease in the number of the monocyte/macrophage-lineage by clodronate-liposomes to attenuate the bone metastasis and growth by cancer cells.

In the present study, using an animal model of bone metastasis with the human lung cancer cell line HARA-B, we investigated whether the administration of clodronate-liposomes was able to modulate bone metastasis by lung cancer cells.[3,20] On the basis of our results, we discuss whether liposome-encapsulated bisphosphonate may be useful for treating not only bone metastasis from lung cancer, but also metastasis in other tissues/organs.

Materials and Methods

Cell culture. HARA-B cells were established from bone metastasis of human lung cancer in nude mice and cultured in RPMI-1640 supplemented with 10% FBS and 10-U/mL

[7]To whom correspondence should be addressed.
E-mail: khiraoka@med.kurume-u.ac.jp

Abbreviations: Ab, antibody; BSA, bovine serum albumin; Cl_2MDP-LIP, clodronate encapsulated by liposomes; DAPI, 4′,6-diamidino-2-phenylindole; FITC, fluorescein-isothiocyanate; HRP, horseradish peroxidase; OCT, optimal cutting temperature; PBS, phosphate-buffered saline; PE, phycoerythrin; PTHrP, parathyroid hormone-related protein; RT, room temperature; TAMs, tumor-associated macrophages; TRAP, tartrate-resistant acid phosphatase.

doi: 10.1111/j.1349-7006.2008.00880.x

penicillin-streptomycin.[3,20] The cells were incubated at 37°C in a humidified atmosphere of 5% CO_2 in air. Human macrophage-like cell line U937 was purchased from the American Type Culture collection (Manassas, VA, USA) and cultured in RPMI supplemented with 10% FBS.

Reagents. FITC-conjugated anti-F4/80 mAb and PE-conjugated anti-CD11b mAb were obtained from CALTAG Laboratories (Burlingame, CA, USA). Rat antimouse F4/80 Ab (MAC497R) was obtained from Serotec (Raleigh, NC, USA). Rat antimouse Gr-1 was purchased from R&D Systems (Minneapolis, MN, USA). Phosphatidylcholine, cholesterol, and clodronate (dichloromethylene diphosphate; Cl_2MDP) were from Sigma-Aldrich (St. Louis, MO, USA). Reveromycin A was a gift from Riken (Saitama, Japan).

Preparation of Cl2MDP-LIP. Cl_2MDP-LIP was prepared as described previously.[12,21] A total of 11 mg of cholesterol and 75 mg of phosphatidylcholine were combined with 10 mL of 0.7-M Cl_2MDP solution and sonicated gently. The resulting liposomes were washed three times to eliminate any free drug. Empty liposomes were prepared as a control under the same conditions using PBS instead of Cl_2MDP.

Animals. Female 5-week-old BALB/C nude mice were obtained from Clea Japan (Tokyo, Japan) and maintained in a specific pathogen-free environment throughout the experiment.

Flow cytometry. Blood samples were obtained from the left cardiac ventricle in mice under anesthesia at day 0, 1, and 2 after stimulation with Cl_2MDP-LIP. A total of 50 mL of each sample was stained for 15 min in a dark doom with FITC-anti-F4/80 mAb (1:50) to label macrophages, and with PE-anti-CD11b mAb (1:50) to label macrophages and neutrophils. Positive cells were measured using a FACScan (Becton Dickinson, USA).[12]

Bone and muscle metastasis by cancer cells, and antimetastatic therapeutic protocol. HARA-B cells (2×10^5/100 μL) were injected into the left cardiac ventricle of mice on day 0 under anesthesia with pentobarbital (0.05 mg/g body weight; Dainippon Pharmaceutical, Osaka, Japan).[3] To assess the inhibitory effect of Cl_2MDP-LIP on the formation of bone and muscle metastasis, Cl_2MDP-LIP at 200 μL or 400 μL was subcutaneously (s.c.) administered into the base of the tail once every 3 days for 6 weeks after the inoculation of HARA-B cells. A subcutaneous administration of reveromycin A (10 mg/kg) was also performed every day for 6 weeks after the inoculation of HARA-B cells. Bone metastases were determined on X-ray photographs at 4 or 6 weeks. Osteolytic bone metastasis on X-ray photographs was evaluated independently. Mice were sacrificed under anesthesia with pentobarbital (0.5 mg/g body weight) at 5 or 6 weeks after inoculation. The extremities and spine were harvested and fixed in 10% formalin. The bone specimens were decalcified in 10% EDTA solution for 1 week and then embedded in paraffin. Tumor metastases were histologically evaluated by the number of colonies and the tumor area in bone and muscle after hematoxylin–eosin staining.[22]

Immunohistochemical and immunofluorescence analysis. Macrophages in bone marrow and tumors were determined using immunohistochemistry for F4/80. Slides were deparaffinized and hydrated, and then rinsed twice with PBS. After 1 h of blocking with 2% goat serum, the sections were incubated overnight with rat antimouse F4/80 (1:200) at 4°C in 1% BSA in PBS. They were then rinsed three times with PBS and treated with HRP-conjugated goat antirat IgG (DakoCytomation, CA, USA) and stained using the DakoCytomation LSAB2 SYSTEM HRP kit, according to the instructions. The sections were counterstained with diluted hematoxylin according to the manufacturer's directions.

For the detection of osteoclasts, TRAP staining was done using a Sigma Diagnostics Acid Phosphatase kit. The number of TRAP-positive cells in bone marrow was counted by microscopy in five random fields in each of three sections at ×200 magnification.

To determine the macrophages and neutrophils in HARA-B tumors, immunofluorescence staining was performed. The tumor samples from bone or muscle were excised and immersed in OCT compound, and immediately frozen in liquid nitrogen. Frozen sections 5-μm thick were prepared. The sections were rinsed with PBS and briefly fixed in 4% paraformaldehyde/PBS for 20 min at RT, followed by two further rinses in PBS. After 1 h of blocking with 2% goat serum, the sections were incubated overnight with rat antimouse $F_{4/80}$ (1:200) or rat antimouse Gr-1 (1:200) at 4°C in 1% BSA in PBS. They were then rinsed three times with PBS and incubated with goat antirat IgG; 1-mg/mL Alexa Fluor 488 for F4/80 (Molecular Probes, Eugene, OR, USA) in 1% BSA in PBS for 60 min at RT. Nuclear staining was carried out using DAPI (1:1000; Dojindo, Japan). Coverslips were mounted on sections using gel mount and viewed using an Olympus BX51 florescence microscope (Olympus, Tokyo, Japan) fitted with an Olympus DP-70 digital camera (Olympus). For quantification, the number of stained cells was counted in five random fields in each of three tumors at ×200 magnification.

Cell survival assay. Cell survival assay was carried out using a Cell Counting Kit (Wako Pure Chemical Industries, Osaka, Japan). In brief, HARA-B cells and human monocytes were plated in triplicate in 96-well plates at a density of 5000 cells/well in basal medium. Following overnight culture, PBS-LIP, Cl_2MDP-LIP, or reveromycin A was added to each concentration, and the cells were incubated for 48 h. After 48 h, WST-1 was added and the cells were incubated for a further 1 h. The plates were read at a wavelength of 450 nm using a microplate reader (Model 3550; Bio-Rad, Richmond, CA, USA). Results are presented as the mean ± SD.

Statistical analysis. The significance of tumor incidence was determined by χ^2-test. The significance of differences in the number of metastases was determined by the Mann–Whitney *U*-test. The significance of differences in the numbers of TRAP-positive cells and tumor area was estimated using the unpaired Student's *t*-test. *P*-values of <0.05 were considered statistically significant.

Results

Decrease in the number of monocytes/macrophages by Cl_2MDP-LIP *in vitro* and *in vivo*. Blood samples were harvested from the left cardiac ventricles of mice under anesthesia as a control. Subsequently, Cl_2MDP-LIP at 200 μL and 400 μL was s.c. administered into the base of the tail, and a 100-μL blood sample was obtained after 24 and 48 h. Each sample was stained with FITC-anti-F4/80 mAb and PE-anti-CD11b mAb to label macrophages, and double-positive cells were measured using a FACScan. The rate of double-positive staining was about 5–7% before stimulation with Cl_2MDP-LIP. The number of double-positive cells in peripheral blood was decreased significantly at 24 h after stimulation with 400 μL of Cl_2MDP-LIP but had recovered slightly after 48 h. Although stimulation with 200 μL of Cl_2MDP-LIP also suppressed the percentage of monocytes at 24 h, the effect was less marked than that of 400 μL of Cl_2MDP-LIP (Fig. 1a,b). PBS-LIP and reveromycin A did not decrease the number of monocytes in peripheral blood (Fig. 1c). We also compared the effects of Cl_2MDP-LIP and reveromycin A on the survival of lung cancer HARA-B cells and macrophage U937 cells in culture. Survival of cancer cells was specifically inhibited by reveromycin A at both 5 and 10 μg/mL, but Cl_2MDP-LIP had no effect up to 200 μM (Table 1). By contrast, survival of macrophages was blocked only by 20–200 μM Cl_2MDP-LIP, but not by reveromycin A at up to 10 μg/mL (Table 1). Thus, Cl_2MDP-LIP had a more specific effect on

doi: 10.1111/j.1349-7006.2008.00880.x

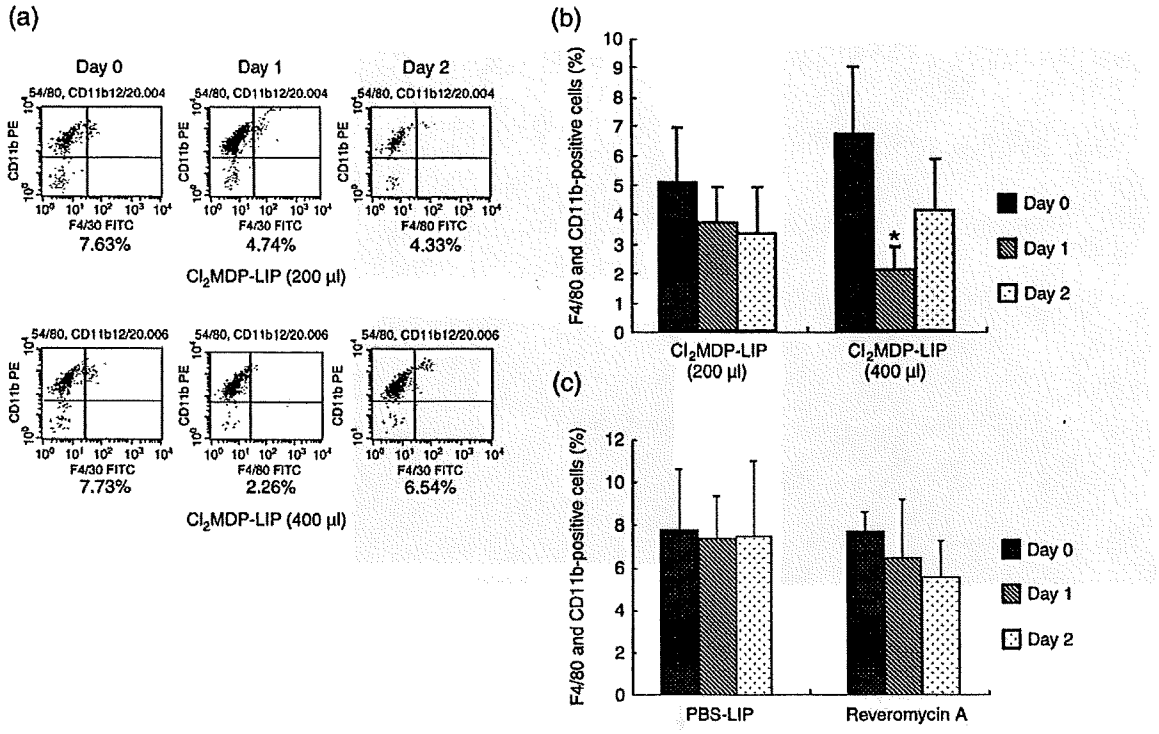

Fig. 1. The decrease in the number of monocytes in peripheral blood by treatment with clodronate encapsulated by liposomes (Cl_2MDP-LIP). (a) FACS analysis of macrophages on days 0, 1, and 2 in peripheral blood of nude mice untreated or treated with Cl_2MDP-LIP. Each blood sample (100 μL) was harvested from the left cardiac ventricle under anesthesia before stimulation. Subsequently, blood samples were taken on days 1 and 2 after the subcutaneous administration of Cl_2MDP-LIP at 200 μL or 400 μL/mouse. Cells were stained with fluorescein-isothiocyanate (FITC)–anti-F4/80 monoclonal antibody (mAb) (1:50) and phycoerythrin (PE)–anti-CD11b mAb (1:50). F4/80- and CD11b-positive cells were measured by FACScan. Upper lane, Cl_2MDP-LIP 200 μL; lower lane, Cl_2MDP-LIP 400 μL. Quantification of the number of monocytes in peripheral blood of nude mice treated with (b) Cl_2MDP-LIP at 200 μL or 400 μL, and (c) PBS-LIP (400 μL) or reveromycin A (10 mg/kg). Each value represents the mean number of monocytes/macrophages ± SD ($n = 4$). *$P < 0.05$.

Table 1. Effect of clodronate, Cl_2MDP-LIP, and reveromycin A on the survival of macrophages and lung cancer cells

Drug	Dose	Lung cancer cells†	Macrophages†
PBS-LIP	0	100.0 ± 4.0	100.0 ± 5.9
Clodronate	2	93.3 ± 5.6	98.3 ± 6.6
	20	93.8 ± 7.1	99.9 ± 11.5
	200 (μM)	99.1 ± 1.8	92.7 ± 8.9
Cl_2MDP-LIP	2	100.0 ± 2.6	94.0 ± 9.1
	20	100.0 ± 0.4	74.7 ± 2.4
	200 (μM)	100.0 ± 5.7	26.4 ± 3.7
Reveromycin A	1	100.0 ± 5.6	101.2 ± 1.6
	5	33.1 ± 2.5	100.7 ± 2.4
	10 (μg/mL)	12.2 ± 0.4 (%)	105.3 ± 1.5 (%)

HARA-B cells (5×10^3/well) and macrophages (5×10^3/well) were incubated for 2 days in the absence or presence of various doses of drugs, and surviving fractions were determined.
Each value was the average of triplicate dishes, and presented as a relative percentage, the cell number in the absence of any drug being taken as 100%. †Mean ± SD.

macrophage survival than reveromycin A in both *in vitro* and *in vivo*.

Inhibition of bone and muscle metastases by Cl2MDP-LIP. Bone and muscle metastases in mice were followed using X-ray photographs at 4 or 6 weeks after inoculation of 2×10^5 cancer cells (Fig. 2a). Colonies of abundant proliferating cancer cells were observed in both bone and muscle when both regions were histologically examined at 6 weeks after cancer cell inoculation (Fig. 2b). We first examined the inhibitory effect of Cl_2MDP-LIP on bone and muscle metastases of cancer cells in comparison with PBS-LIP (control). Based on the effects of Cl_2MDP-LIP (Fig. 1), we determined the protocols shown in Fig. 3a. Cl_2MDP-LIP was administered s.c. at 200 μL and 400 μL once every 3 days for 6 weeks just after the inoculation of cancer cells (Fig. 3a). All of the mice treated with PBS-LIP showed destructive bone changes in X-ray photographs or paralysis in the hind limbs at 6 weeks. By contrast, treatment with Cl_2MDP-LIP at 200 μL and 400 μL inhibited the development of bone metastases by cancer cells (Fig. 3b). Fig. 3b also shows the therapeutic effects of reveromycin A on bone metastasis when administered s.c. at 10 mg/kg daily after cancer cell inoculation. Treatment with reveromycin A markedly inhibited bone metastasis by lung cancer cells. Quantitative analysis showed that both the incidence of bone metastasis and the number of metastatic foci were significantly decreased by treatment with Cl_2MDP-LIP at 200 μL and 400 μL, and reveromycin A (Table 2). The inhibitory effect of Cl_2MDP-LIP at 400 μL was strongest among those agents (Table 2).

We also compared the therapeutic effects of various agents on both muscle metastasis and bone metastasis by histological analysis. Treatment with Cl_2MDP-LIP at 400 μL and reveromycin A significantly decreased the number of tumor colonies in bone (Table 3). We also observed a marked decrease of tumor colony numbers in muscle by Cl_2MDP-LIP at 400 μL ($P < 0.05$) but not by reveromycin A. Furthermore, Cl_2MDP-LIP at 400 μL significantly ($P < 0.05$) inhibited tumor area in bone as compared

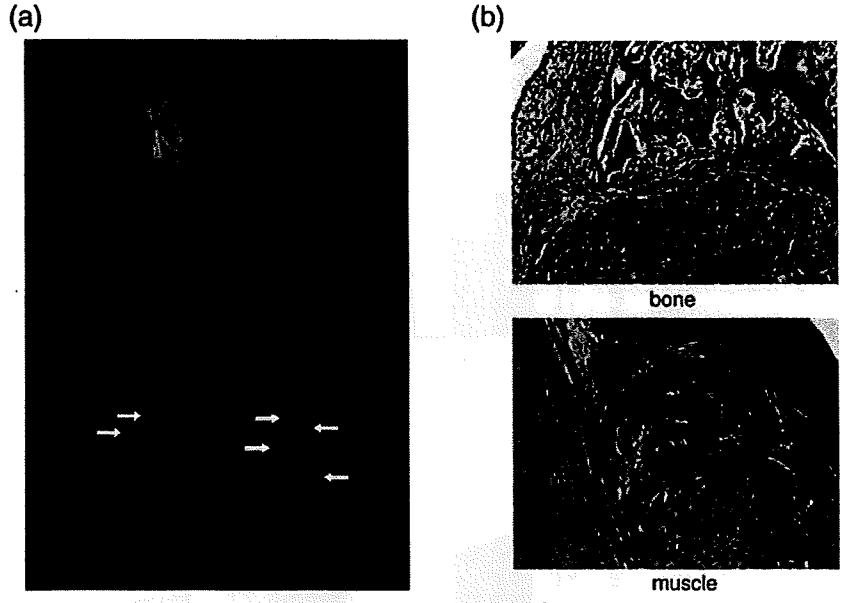

Fig. 2. Radiographic and histological analysis of untreated mice. The human lung cancer cell line HARA-B (2×10^5 cells per mouse) was injected into the left cardiac ventricle of nude mice. (a) Bone metastases were determined by radiography on the indicated days after inoculation. Arrows indicate osteolytic bone metastases. (b) The mice were sacrificed at 6 weeks, and bone and muscle metastases were examined histologically. Bar, 200 μm; T, tumor; B, bone; M, muscle.

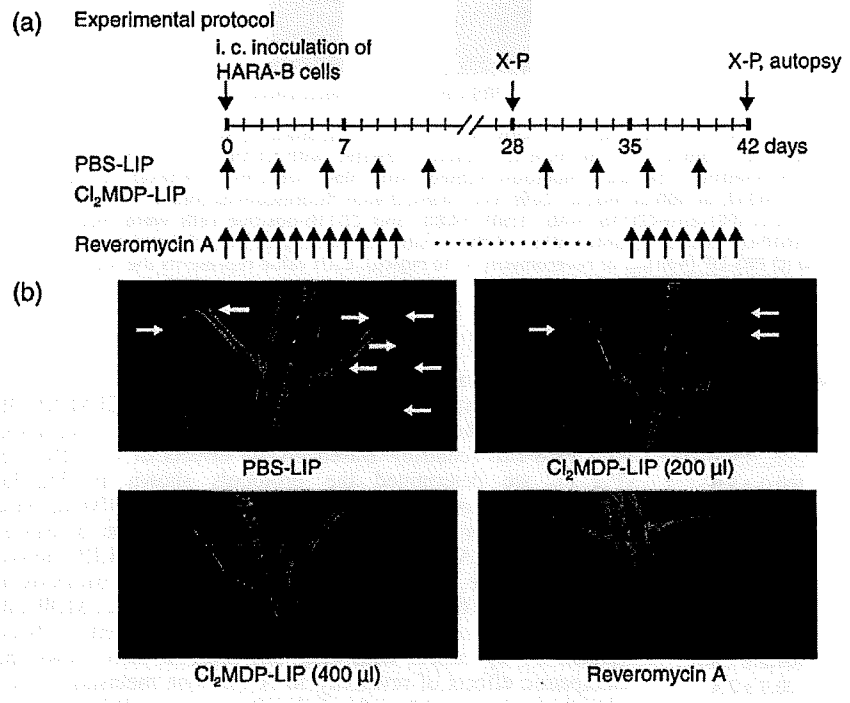

Fig. 3. Clodronate-liposomes and reveromycin A decreased the frequency of bone metastasis by lung cancer cells. (a) Experimental protocol of the treatment with clodronate encapsulated by liposomes (Cl_2MDP-LIP) and reveromycin A on bone or muscle metastases of HARA-B cells. (b) Radiographs of the hind limbs of nude mice treated with PBS-LIP (400 μL), Cl_2MDP-LIP (200 μL), Cl_2MDP-LIP (400 μL), and reveromycin A (10 mg/kg). HARA-B cells (2×10^5 per mouse) were injected into the left cardiac ventricle. At 6 weeks after the subcutaneous administration of PBS-LIP, Cl_2MDP-LIP (200 μL and 400 μL/mouse once every 3 days), and reveromycin A (every day) the extent of bone and muscle metastases was determined by radiography and autopsy. Arrows indicate osteolytic bone metastases.

Table 2. Radiological analysis of inhibitory effects of clodronate-liposomes and reveromycin A on bone metastasis

Treatment	Incidence of bone metastasis	No. of metastatic foci*
PBS-LIP	8/9	6.6 ± 4.2
Cl_2MDP-LIP (200 μl)	3/7†	0.9 ± 1.2‡
Cl_2MDP-LIP (400 μl)	1/9‡	0.1 ± 0.3‡
Reveromycin A	1/9‡	0.3 ± 1.0‡

HARA-B cells (2×10^5 per mouse) were injected into the left cardiac ventricle of nude mice on day 0. The mice were s.c. administered PBS-LIP, Cl_2MDP-LIP (200 and 400 μl/mouse once every three days), or reveromycin A (10 mg/kg daily) from day 0 to 6 weeks. Bone metastases were determined by radiographs at 4 and 6 weeks after inoculation. *Mean ±SD, †$P < 0.05$, ‡$P < 0.01$.

with the control, whereas reveromycin A or Cl_2MDP-LIP at 200 μL decreased the tumor area by only 30–50% compared with the control. In contrast, there was no significant difference in the inhibitory effect on tumor area in muscle between the untreated control and treated groups. Of the various treatments against tumor area in muscle, only Cl_2MDP-LIP at 400 μL had an inhibitory effect, although the inhibition was not statistically significant (Table 3).

Decrease in the number of both macrophages in tumor and osteoclasts in bone by Cl2MDP-LIP. We examined whether the number of macrophages was affected by treatment with Cl_2MDP-LIP. The number of macrophages in tumors was also estimated by immunofluorescence analysis with a rat antimouse F4/80 antibody. The immunofluorescence analysis of mice

doi: 10.1111/j.1349-7006.2008.00880.x

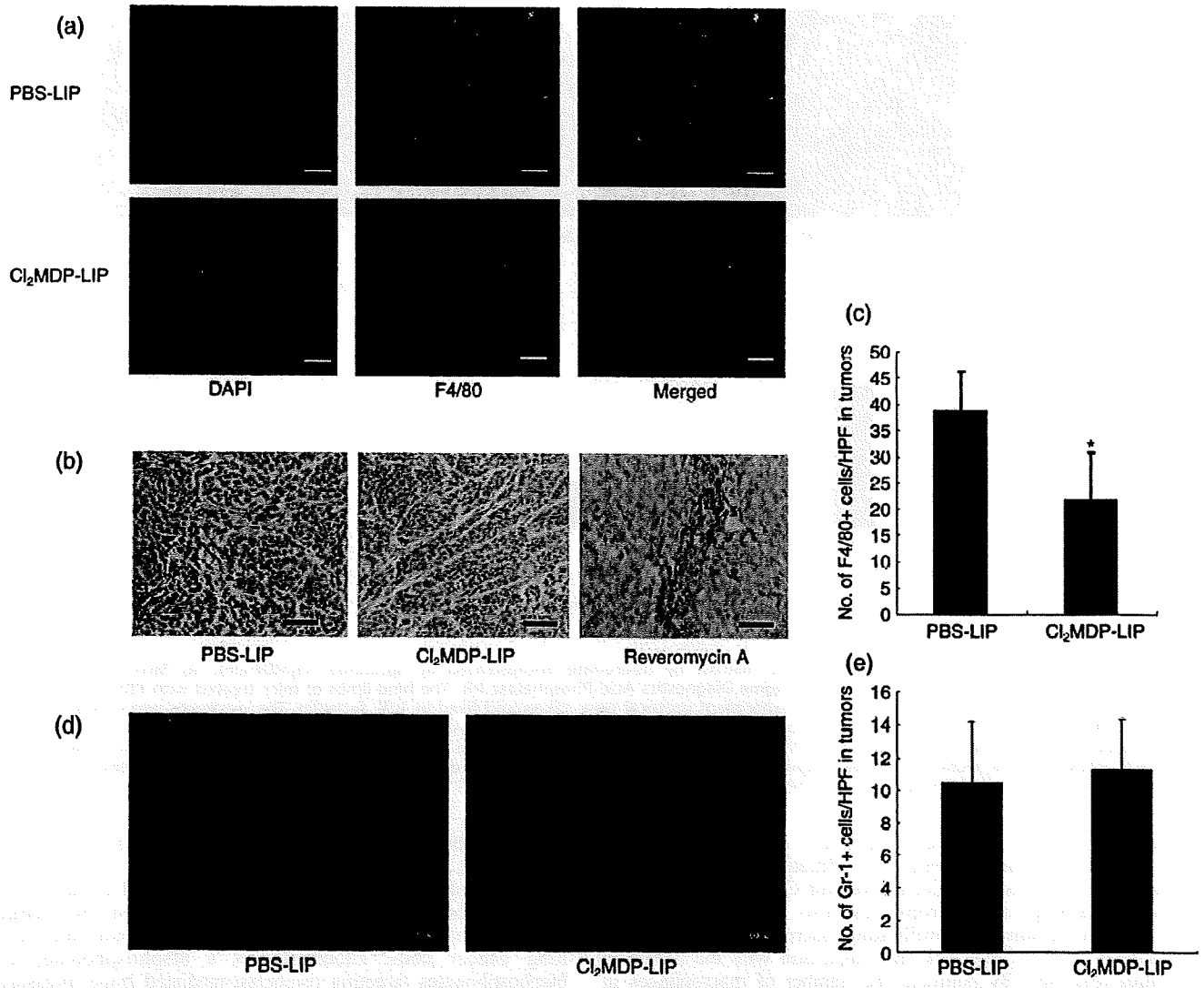

Fig. 4. Reduced infiltration of macrophages in tumors by clodronate encapsulated by liposomes (Cl_2MDP-LIP). (a) Immunofluorescence analysis of F4/80-positive cells in HARA-B tumors. The tumors derived from mice treated with PBS-LIP, Cl_2MDP-LIP (400 μL), and reveromycin A (10 mg/kg) were excised at 6 weeks after inoculation as described in the experiment protocol. The samples were stained with rat anti-F4/80 antibody (1:200), and ant-rat Alexa-Fluor-488 (1:1000) was used as secondary antibody to detect the F4/80-positive macrophages. Nuclear staining was carried out using 4′,6-diamidino-2-phenylindole (DAPI) (1:1000) to present profiles of tumor masses, and the merged figures were used to localize the F4/80-positive cells in tumor masses. (b) Some sections were incubated with rat anti-F4/80 antibody and horseradish peroxidase (HRP)–conjugated goat antirat IgG was used as secondary antibody. Bar, 100 μm. (c) Quantification of macrophages in HARA-B tumors. The number of stained cells was counted in five random fields for each of three tumors derived from mice treated with PBS-LIP and Cl_2MDP-LIP at ×200 magnification. Each value represents the mean number of macrophages ± SD. $^*P < 0.05$. (d) Some sections were incubated with rat anti-Gr-1 antibody. Bar, 100 μm. (e) Quantification of neutrophiles in HARA-B tumors. The number of stained cells was counted in five random fields for each of three tumors at ×200 magnification. Each value represents the mean number of neutrophiles ± SD.

Table 3. Histological analysis of inhibitory effects of clodronate-liposomes and reveromycin A on bone metastasis

Treatment	Incidence of metastasis	No. of tumor colonies*		Tumor area (mm^2)*	
		bone	muscle	bone	muscle
PBS-LIP	8/9	4.7 ± 4.1	13.2 ± 14.1	8.1 ± 6.9	16.4 ± 20.2
Cl_2MDP-LIP (200 μl)	5/7	2.0 ± 3.0	7.9 ± 13.1	5.6 ± 9.3	10.1 ± 11.3
Cl_2MDP-LIP (400 μl)	5/9	0.4 ± 0.7†	1.2 ± 1.2†	0.4 ± 0.8†	2.0 ± 3.3
Reveromycin A	6/9	0.7 ± 1.3†	4.3 ± 4.6	3.7 ± 9.2	14.9 ± 13.9

HARA-B cells (2×10^5 per mouse) were injected into the left cardiac ventricle of nude mice on day 0. The mice were s.c. administered PBS-LIP, Cl_2MDP-LIP (200 and 400 μl/mouse once every three days), or reveromycin A (10 mg/kg daily) from day 0 to 6 weeks. The mice were sacrificed at 6 weeks and the formation of metastasis in bone or muscle was examined. The tumor area is represented as the sum of the individual tumor areas in bone or muscle of each mouse calculated as $\pi d^2/4$, where d is the diameter of each tumor in mm. *Mean ± SD, †$P < 0.05$.

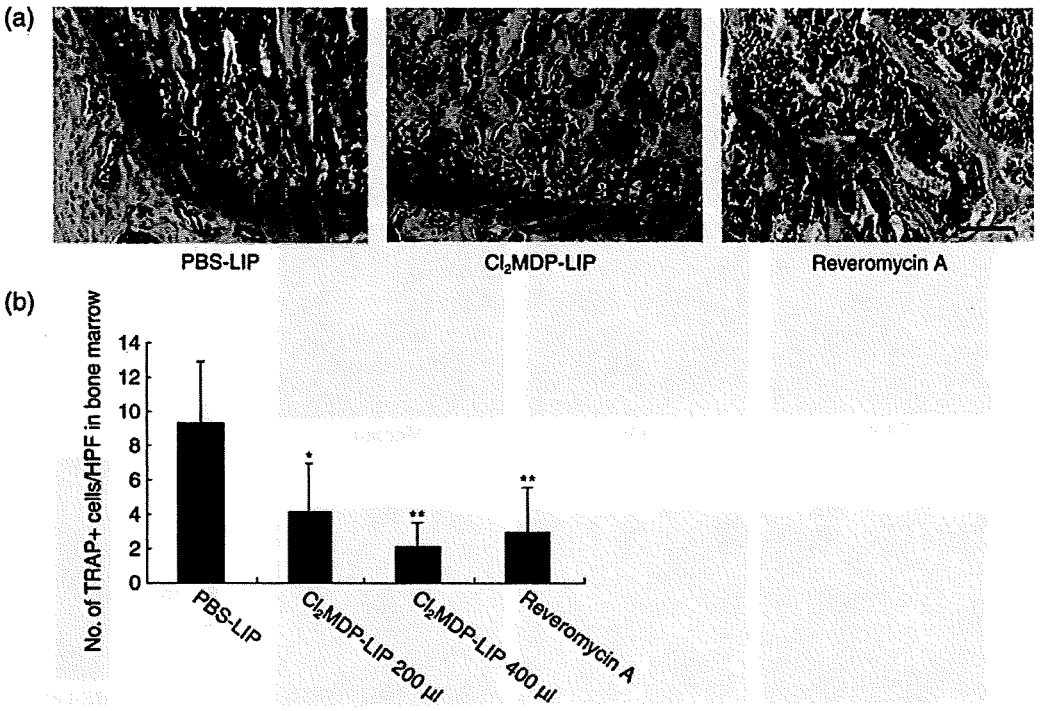

Fig. 5. Reduced number of osteoclasts in bone marrow by clodronate encapsulated by liposomes (Cl_2MDP-LIP). (a) Tartrate-resistant acid phosphatase (TRAP) staining was done using a Sigma Diagnostics Acid Phosphatase kit. The hind limbs of mice treated with PBS-LIP, Cl_2MDP-LIP (200 μL and 400 μL), and reveromycin A in the experiment protocol were taken and fixed in 10% formalin. The specimens were decalcified in a 10% EDTA solution for 1 week and then embedded in paraffin. Arrows indicate TRAP-positive osteoclasts in bone marrow. Bar, 100 μm. (b) Quantification of osteoclasts in bone marrow. The number of TRAP-positive cells in bone marrow was counted under a microscope in five random fields in each of three sections at ×200 magnification. The statistical significance of differences between the controls and other groups was analyzed using the unpaired Student's *t*-test. $*P < 0.05$, $**P < 0.01$.

treated with PBS-LIP revealed numerous macrophages stained with F4/80 in tumors, whereas infiltrating macrophages in tumors were decreased in mice treated with Cl_2MDP-LIP (Fig. 4a). Immunostaining of macrophages also showed a marked decrease in the number of infiltrating macrophages in tumors on treatment with Cl_2MDP-LIP in comparison with the untreated control (Fig. 4b). By contrast, the number of macrophages in bone marrow was not affected by treatment with Cl_2MDP-LIP (data not shown). Quantitative analysis showed a significant decrease of infiltrating macrophages in tumors after treatment with Cl_2MDP-LIP (Fig. 4c). The number of neutrophils in tumors was not affected by treatment with Cl_2MDP-LIP in comparison with the untreated control (Fig. 4d,e).

We further examined whether treatment with Cl_2MDP-LIP at 400 μL as well as reveromycin A affected the number of osteoclasts in bone marrow. The hind limbs of mice treated with PBS-LIP, Cl_2MDP-LIP, and reveromycin A were harvested at 6 weeks after inoculation, and osteoclasts were identified by TRAP staining (Fig. 5a). We observed many TRAP-positive osteoclasts in control mice with bone metastasis. By contrast, the number of osteoclasts was decreased in reveromycin A– and Cl_2MDP-LIP-treated mice. Quantitative analysis demonstrated that the number of osteoclasts was significantly decreased in bone marrow by Cl_2MDP-LIP at 400 μL and by reveromycin A in comparison with the controls (Fig. 5b).

Discussion

In the present study, we assessed the effect of a decreasing number of monocytes/macrophages in peripheral blood and the tumor stroma on bone and muscle metastases using an experimental bone metastasis model in nude mice inoculated with human lung cancer cells which showed strong bone metastasis activity.[3,20] Clodronate-liposomes reduced the number of monocytes in peripheral blood as well as the number of osteoclasts in bone marrow, accompanied by marked inhibition of metastasis to both bone and skeletal muscle by lung cancer cells. Clodronate is a bisphosphonate, and bisphosphonates targeting osteoclast-mediated bone metastasis have been used to treat bone metastasis.[23] The underlying mechanism of their effects is inhibition of a key enzyme in the mevalonate pathway, farnesyl diphosphate synthase, resulting in prevention of protein phenylation and Ras activation, and also producing a unique adenosine triphosphate analog (Apppi), resulting in induction of apoptosis of both osteoclasts and cancer cells.[23] Clodronate encapsulated by liposomes has been developed and successfully applied in several studies for depletion of macrophages.[12,13,21] Although free clodronate is not ingested by macrophages and is rapidly removed from circulation,[24] the liposome-encapsulated form is phagocytosed, and intracellular release of clodronate promotes apoptosis.[21]

Treatment with the osteoclast-targeting agent reveromycin A also significantly decreased bone metastasis by lung cancer cells. Reveromycin A, a novel antibiotic, inhibits bone resorption by inducing the specific apoptosis of activated osteoclasts, possibly because reveromycin A is specifically transported into osteoclasts at acidic pH.[25–27] In this study, histological analyses showed that reveromycin A markedly decreased the number of osteoclasts in bone lesions, suggesting that reveromycin A specifically inhibits osteolytic bone metastasis by targeting osteoclasts in bone lesions. Reveromycin A only slightly inhibited the number of muscle metastases, perhaps through its direct inhibition of cancer cell survival. By contrast, clodronate-liposomes inhibited the survival of macrophages in culture,

doi: 10.1111/j.1349-7006.2008.00880.x

whereas reveromycin A did not. These findings suggest that the clodronate-liposome-induced inhibition of both bone and muscle metastasis may be due to a reduction the number of not only osteoclasts, but also macrophages infiltrating the metastatic lesions in both bone and muscle.

Monocytes in peripheral blood are versatile precursors with the potential to differentiate into the various types of specialized macrophages.[28] Macrophages in the tumor environment are activated by inflammatory responses during the acquisition of malignant characteristics in both the primary tumor and bone metastases.[6] Infiltrating macrophages under conditions of inflammation are derived mainly from peripheral blood monocytes, and create conditions in the tumor stroma and bone metastases that favor metastasis/invasion and angiogenesis through the production of various chemokines, cytokines, growth factors, proteases, and hypoxia.[7–9] Clodronate-liposomes have been shown to significantly reduce the number of monocytes in peripheral blood *in vivo*[12] (see also Fig. 1), and the survival of macrophages *in vitro*. Treatment with clodronate-liposomes also markedly inhibits inflammatory cytokine-induced angiogenesis and infiltration of monocytes/macrophages in the cornea,[12] and also tumor growth by lung cancer cells.[14] Thus, a decrease in the number of macrophages by clodronate-liposomes might also block the metastasis of cancer cells to bone.

Tumor angiogenesis is often closely associated with bone metastasis by cancer cells,[15,29] possibly through angiogenesis in the tumor stroma and also in the metastases themselves. Activation of the *VEGF*, *IL-8*, *bFGF*, and *cyclooxygenase-2* genes in both tumor cells and macrophages in the tumor stroma by inflammatory cytokines induces angiogenesis.[12,30] It has been reported that synergistic interaction between macrophages and tumor cells is required for tumor cell migration through a paracrine loop involving reciprocal signaling of EGF and colony-stimulating factor-1.[31] Inflammatory cytokines produced by macrophages affect tumor invasion and angiogenesis, suggesting that the recruitment of macrophages into the tumor stroma is prerequisite for the acquisition of malignant characteristics.[4–6,9] Previous studies have demonstrated the apparent involvement of macrophages in inflammatory cytokine-induced angiogenesis[12] and also in tumor-induced angiogenesis.[13] The blocking of bone metastasis from lung cancer might be due in part to decreased macrophage-induced angiogenesis. However it still remains to be clarified how bone metastasis is linked to angiogenesis in metastatic lesions.

Treatment with clodronate-liposomes markedly inhibited the metastasis of cancer cells to muscle as well as bone. However, whether a decrease in the number of macrophages by this drug is directly involved in its inhibitory effect on the metastasis to muscle needs to be further studied. Jones *et al.* have recently reported that bone metastasis after the intracardiac injection of melanoma cells is dependent on RANK/RANKL signaling.[32] However, in our present study, the role of RANK/RANKL signaling was not examined. Regarding the pleiotropic mechanisms of bone metastasis by cancer cells, we consider it likely that macrophage lineages provide a microenvironment that is favorable for metastasis and tumor growth not only in bone but also in muscle.[33] The inhibition of metastasis in both bone and muscle by clodronate-liposomes might be due to depletion of osteoclasts precursors as well as tumor-associated macrophages.

In conclusion, osteoclasts are well known to play pivotal roles in bone metastasis by cancer cells, and osteoclasts are derived from monocytes/macrophages. Bisphosphonates are most frequently used to treat bone metastasis in cancer patients, and act by possibly targeting osteoclasts and cancer cells.[34] The present study demonstrated that treatment with a bisphosphonate encapsulated by liposomes markedly decreased both bone and muscle metastases by lung cancer cells. In contrast, treatment with the osteoclast-targeting drug, reveromycin A, specifically inhibited bone metastasis, but not muscle metastasis, by lung cancer cells. These findings suggest that bisphosphonates encapsulated by liposomes may be a novel and potent therapeutic agent against not only bone metastasis but also other organ metastases of lung cancer cells in humans.

Acknowledgments

We thank Kazuhiro Yoshida, Hiromi Kuboyama, and Hitomi Wakita for technical assistance. This study was partly supported by the 21st Century COE Program for Medical Science; a grant-in-aid for the 3rd term comprehensive 10-year strategy for cancer control from the Ministry of Health, Welfare (M.K.), and Labor of Japan; and the Innovation Center for Medical Redox Navigation, Kyushu University (M.O., M.K.).

References

1 Fidler IJ, Radinsky R. Genetic control of cancer metastasis. *J Natl Cancer Inst* 1990; **82**: 166–8.
2 Guise TA. Molecular mechanism of osteolytic bone metastasis. *Cancer* 2000; **88**: 2892–8.
3 Iguch H, Tanaka S, Ozawa Y *et al.* An experimental model of bone metastasis by human lung cancer cells: the role of parathyroid hormone-related protein in bone metastasis. *Cancer Res* 1996; **56**: 4040–3.
4 Balkwill F, Mantovani A. Inflammation and cancer: back to Vichow? *Lancet* 2001; **357**: 539–45.
5 Coussens LM, Werb Z. Inflammation and cancer. *Nature* 2002; **420**: 860–7.
6 Pollard JW. Tumor-educated macrophages promote tumor progression and metastasis. *Nat Rev Cancer* 2004; **4**: 71–8.
7 Polverini PJ, Cotran PS, Gimbrone MA Jr, Unanue ER. Activated macrophages induce vascular proliferation. *Nature* 1977; **269**: 804–6.
8 Mantovani A, Allavena P, Sica A. Tumor-associated macrphages as a prototypic type II plarised phagocytic population: role in tumor progression. *Eur J Cancer* 2004; **40**: 1660–7.
9 Kuwano M, Basaki Y, Kuwano T *et al.* The critical role of inflammatory cell infiltration in tumor angiogenesis – a target for antitumor drug development? In: *New Angiogenesis Research*. New York: Nova Science Publishers, Inc, 2005; 157–70.
10 Sunderkotter C, Steinbrink K, Goebeler M, Bhardwaj R, Sorg C. Macrophages and angiogenesis. *J Leukoc Biol* 1994; **55**: 410–22.
11 Leek RD, Lewis CE, Whitehouse R, Greenall M, Clarke J, Harris AL. Association of macrophage infiltration with angiogenesis and prognosis in invasive breast carcinoma. *Cancer Res* 1996; **56**: 4625–9.
12 Nakao S, Kuwano T, Tsutsumi-Miyahara C *et al.* Infiltration of COX2-expressiong macrophages is prerequisite for IL-1b-induced neovascularization and tumor growth. *J Clinic Invest* 2005; **115**: 2979–91.
13 Zeisberger SM, Odermatt B, Marty C, Zehnder-Fjallman AHM, Ballmer-Hofer K, Schwendener RA. Clodronate-liposome-mediated depletion of tumor-associated macrophages: a new and highly effective antiangiogenic therapy approach. *Br J Cancer* 2006; **95**: 272–81.
14 Kimura Y, Watari K, Fotovati A *et al.* Inflammatory stimuli from macrophages and cancer cells synergistically promote tumor growth and angiogenesis. *Cancer Sci* 2007; **98**: 2009–18.
15 Ribatti .D, Nico B, Vacca A. Importance of the bone marrow microenvironment in inducing the angiogenic response in multiple myeloma. *Oncogene* 2006; **25**: 4257–66.
16 Gardner CR. Morphological analysis of osteoclastogenesis induced by RANKL in mouse bone marrow cell cultures. *Cell Biol Int* 2007; **31**: 672–82.
17 Gallwitz WE, Guise TA, Mundy GR. Guanosine nucleotides inhibit different syndromes of PTHrP excess caused by human cancers *in vivo*. *J Clin Invest* 2002; **110**: 1559–72.
18 Guise TA, Yin JJ, Taylor SD *et al.* Evidence for a causal role of parathyroid hormone-related protein in the pathogenesis of human breast cancer-mediated osteolysis. *J Clin Invest* 1996; **98**: 1544–9.
19 Mundy GR. Metastasis to bone: causes, consequences and therapeutic opportunities. *Nat Rev Cancer* 2002; **2**: 584–93.
20 Iguchi H, Ono M, Matsushima K, Kuwano M. Overproduction of IL-8 results in suppression of bone metastasis by lung cancer cells *in vivo*. *Int J Oncol* 2000; **17**: 329–33.
21 Van Rooijen N. The liposome-mediated macrophage 'suicide' technique. *J Immunol Meth* 1989; **124**: 1–6.

22 Koshkina NV, Kleinerman ES. Aerosol gemcitabine inhibits the growth of primary osteosarcoma and osteosarcoma lung metastases. *Int J Cancer* 2005; **116**: 458–63.
23 Green JR. Bisphosphonates: preclinical review. *Oncologist* 2004; **9** (Suppl 4): 3–13.
24 Fleisch H. Bisphosphonates: a new class of drugs in disease of bone and calcium metabolism. *Handbook Exp Pharmacol* 1988; **83**: 441.
25 Osada H, Koshino H, Isono K, Takahashi H, Kawanishi G. Reveromycin A, a new antibiotic which inhibits the mitogenic activity of epidermal growth factor. *J Antibiot* 1991; **44**: 259–61.
26 Muguruma H, Yano S, Kakiuchi S *et al.* Reveromycin A inhibits osteolytic bone metastasis of small-cell lung cancer cells, SBC-5, through an antiosteoclastic activity. *Clin Cancer Res* 2005; **11**: 8822–8.
27 Woo JT, Kawatani M, Kato M *et al.* Reveromycin A, an agent for osteoporosis, inhibits bone resorption by inducing apoptosis specifically in osteoclasts. *Proc Natl Acad Sci USA* 2006; **103**: 4729–34.
28 Luo Y, Zhou H, Krueger J *et al.* Targeting tumor-associated macrophages as a novel strategy against breast cancer. *J Clin Invest* 2006; **116**: 2132–41.
29 Muguruma H, Matsumori Y *et al.* Antitumor vascular strategy for controlling experimental metastatic spread of human small-cell lung cancer cells with ZD6474 in natural killer cell-depleted severe combined immunodeficient mice. *Clin Cancer Res* 2005; **11**: 8789–98.
30 Torisu H, Ono M, Kiryu H *et al.* Macrophage infiltration correlates with tumor stage and angiogenesis in human malignant melanoma: possible involvement of TNF alpha and IL-1 alpha. *Int J Cancer* 2000; **85**: 182–8.
31 Wyckoff J, Wang W, Lin EY *et al.* A paracrine loop between tumor cells and macrophages is required for tumor cell migration in mammary tumors. *Cancer Res* 2004; **64**: 7022–9.
32 Jones DH, Nakashima T, Sanchez OH *et al.* Regulation of cancer cell migration and bone metastasis by RANKL. *Nature* 2006; **440**: 692–6.
33 Ono M. Molecular links between tumor angiogenesis and inflammation: inflammatory stimuli of macrophages and cancer cells as targets for therapeutic strategy. *Cancer Sci* 2008; in press.
34 Green JR, Clezardin P. Mechanisms of bisphosphonate effects on osteoclasts, tumor cell growth, and metastasis. *Am J Clin Oncol* 2002; **25**: S3–9.

doi: 10.1111/j.1349-7006.2008.00880.x

Expression of HER2 and Estrogen Receptor α Depends upon Nuclear Localization of Y-Box Binding Protein-1 in Human Breast Cancers

Teruhiko Fujii,[1,3,5] Akihiko Kawahara,[1,4] Yuji Basaki,[6] Satoshi Hattori,[2] Kazutaka Nakashima,[1,4] Kenji Nakano,[1] Kazuo Shirouzu,[3] Kimitoshi Kohno,[7] Takashi Yanagawa,[2] Hideaki Yamana,[1,3] Kazuto Nishio,[8] Mayumi Ono,[6] Michihiko Kuwano,[1] and Masayoshi Kage[1,4]

[1]Center for Innovative Cancer Therapy of the 21st Century Center of Excellence Program for Medical Science; [2]Biostatistics Center, Kurume University; [3]Department of Surgery, Kurume University School of Medicine; [4]Department of Pathology, Kurume University Hospital, Kurume, Japan; [5]National Hospital Organization Kyushu Medical Cancer; [6]Department of Pharmaceutical Oncology, Graduate School of Pharmaceutical Sciences, Kyushu University, Fukuoka, Japan; [7]Department of Molecular Biology, University of Occupation and Environmental Health, Kitakyushu, Japan; and [8]Department of Genome Biology, Kinki University School of Medicine, Osakasayama, Japan

Abstract

In our present study, we examined whether nuclear localization of Y-box binding protein-1 (YB-1) is associated with the expression of epidermal growth factor receptors (EGFR), hormone receptors, and other molecules affecting breast cancer prognosis. The expression of nuclear YB-1, clinicopathologic findings, and molecular markers [EGFR, HER2, estrogen receptor (ER)α, ERβ, progesterone receptor, chemokine (C-X-C motif) receptor 4 (CXCR4), phosphorylated Akt, and major vault protein/lung resistance protein] were immunohistochemically analyzed. The association of the expression of nuclear YB-1 and the molecular markers was examined in breast cancer cell lines using microarrays, quantitative real-time PCR, and Western blot analyses. Knockdown of YB-1 with siRNA significantly reduced EGFR, HER2, and ERα expression in ERα-positive, but not ERα-negative, breast cancer cell lines. Nuclear YB-1 expression was positively correlated with HER2 (P = 0.0153) and negatively correlated with ERα (P = 0.0122) and CXCR4 (P = 0.0166) in human breast cancer clinical specimens but was not correlated with EGFR expression. Nuclear YB-1 expression was an independent prognostic factor for overall (P = 0.0139) and progression-free (P = 0.0280) survival. In conclusion, nuclear YB-1 expression might be essential for the acquisition of malignant characteristics via HER2-Akt–dependent pathways in breast cancer patients. The nuclear localization of YB-1 could be an important therapeutic target against not only multidrug resistance but also tumor growth dependent on HER2 and ERα. [Cancer Res 2008;68(5):1504–12]

Introduction

Nuclear localization of Y-box binding protein-1 (YB-1) is required for its transcriptional control of multidrug resistance–related genes and for its action in repairing DNA damage induced by anticancer agents and radiation in cancer cells; as a result of these actions, it is responsible for the acquisition of global drug resistance to a wide range of anticancer agents (1, 2). Immunohistochemical analyses have shown that nuclear YB-1 localization is a target marker of intrinsic importance for global drug resistance in cancer (2). Bargou et al. (3) reported that nuclear localization of YB-1 was associated with P-glycoprotein expression in human primary breast cancers, and other immunohistochemical studies have shown an association between YB-1 and P-glycoprotein in osteosarcoma, synovial sarcoma, breast cancer, ovarian cancer, and prostate cancer (4–12). Fujita et al. (13) reported that the increase in P-glycoprotein expression when patients were treated with paclitaxel was accompanied by nuclear YB-1 localization in breast cancers.

Nuclear expression of YB-1 is often associated with poor prognosis in various human malignancies, including breast cancer (3, 6), ovarian cancer (8, 11), synovial sarcoma (5), and lung cancer (14). In a study using molecular profiling, Faury et al. (15) recently showed that overexpression of YB-1 is a novel prognostic target for pediatric glioblastoma; however, the intracellular localization of YB-1 was not determined. These clinical studies suggest the close involvement of YB-1 in the acquisition of global drug resistance (2); however, it remains unclear whether the association of YB-1 with poor prognosis is due to this effect, as YB-1 nuclear localization is also a prognostic marker irrespective of P-glycoprotein expression (8, 14, 16). This suggests that other factors affecting tumor growth, invasion, and metastasis could also be involved in the association of YB-1 with poor prognosis in malignant cancers (8, 14).

YB-1 gene induced the development of breast cancers of many histologic types in an experimental animal model (17), suggesting that YB-1 is oncogenic (18). YB-1 overexpression in human mammary epithelial cells induced epidermal growth factor (EGF)-independent growth by activating the EGF receptor (EGFR) pathway (18). Jurchott et al. (19) reported that nuclear localization of YB-1 was induced during G_1-S phase transition, accompanied by increased expression of cyclin A and B. These studies suggest a close link between YB-1 expression and the growth potential of breast cancer cells, which might contribute to poor prognosis. Wu and colleagues (20) established a close correlation between YB-1 expression and the expression of EGFR and HER2 in breast cancer patients (n = 389) using tumor tissue arrays. Knock-out of YB-1 in mice caused some embryonic lethality, severe growth retardation, and exencephaly (21, 22). Moreover, fibroblasts derived from YB-$1^{-/-}$ knockout embryos had slower growth rates than those from wild-type embryos, and failed to undergo morphologic transformation *in vitro* (22, 23). Sutherland et al. (24) have also shown that breast cancer cells with defective nuclear localization of YB-1 multiply slowly in monolayers and during anchorage-independent growth.

Note: Supplementary data for this article are available at Cancer Research Online (http://cancerres.aacrjournals.org/).

T. Fujii, A. Kawahara, Y. Basaki, and S. Hattori contributed equally to this work.

Requests for reprints: Masayoshi Kage, Department of Pathology, Kurume University Hospital, Kurume 830-0011, Japan. Phone: 81-942-31-7651; Fax: 81-942-31-7651; E-mail: masakage@med.kurume-u.ac.jp.

doi:10.1158/0008-5472.CAN-07-2362

Taken together, these findings suggest that YB-1 plays a key role in the expression of not only drug resistance–related genes but also cell growth–related genes.

In the present study, we determined whether nuclear YB-1 localization influenced the expression of growth factor and hormone receptors, EGFR, HER2, estrogen receptor (ER)α, and ERβ, in human breast cancers. In addition, we used molecular profiling to examine whether nuclear YB-1 localization affected the expressions of major vault protein/lung resistance protein (MVP/LRP), phosphorylated Akt (p-Akt), progesterone receptor (PgR), and chemokine (C_X_C motif) receptor 4 (CXCR4).

Materials and Methods

Cell lines, protein extraction, and immunoblotting. Human breast cancer cell lines, T-47D, MCF-7, KPL-1, MDA-MB231, and SKBR-3 were obtained from the American Type Culture Collection and were grown as described elsewhere (25). Anti–YB-1 was generated as described previously (26). Anti-EGFR and anti-PTEN antibodies were obtained from Cell Signaling Technology. Anti-HER2 was purchased from Upstate, Inc. Anti-ERα was obtained from Santa Cruz Biotechnology, Inc. Anti-CXCR4 was obtained from Abcam plc. Anti– glyceraldehyde-3-phosphate dehydrogenase (GAPDH) was purchased from Trevigen, Inc. Anti-MVP/LRP was a kind gift from Professor S. Akiyama (Kagoshima University, Kagoshima, Japan). LY294002 was obtained from Sigma Co. Trastuzumab was purchased from Chugai Pharmaceutical Company. Cells were lysed in cold protein extraction reagent (M-PER; Pierce) with protease inhibitors and phosphatase inhibitors. Nuclear and cytoplasmic fractions were prepared as described previously (27). Lysates were subjected to SDS-PAGE and blotted onto Immobilon membrane (Millipore Corp.). After transfer, the membrane was incubated with the primary antibody and visualized with secondary antibody coupled to horseradish peroxidase and Supersignal West Pico Chemiluminescent Substrate (Pierce). Bands on Western blots were analyzed densitometrically using Scion Image software (version 4.0.2; Scion Corp.).

Microarray analysis. The small interfering RNA (siRNA) corresponding to nucleotide sequences of YB-1 (5′-GGU UCC CAC CUU ACU ACA U-3′) was purchased from QIAGEN Inc. SiRNA duplexes were transfected using Lipofectamine and Opti-MEM medium (Invitrogen) according to the manufacturer's recommendations. Duplicate samples were prepared for microarray hybridization. Forty-eight hours after siRNA transfection, total RNA was extracted from cell cultures using ISOGEN (Nippon Gene Co. Ltd.). Two micrograms of total RNA were reverse transcribed using GeneChip 3′-Amplification Reagents One-Cycle cDNA Synthesis kit (Affymetrix, Inc.) and then labeled with Cy5 or Cy3. The labeled cRNA was applied to the oligonucleotide microarray (Human Genome U133 Plus 2.0 Array; Affymetrix). The microarray was scanned on a GeneChip Scanner3000, and the image was analyzed using a GeneChip Operating Software ver1.

Quantitative real-time PCR. RNA was reverse transcribed from random hexamers using avian myeloblastosis virus reverse transcriptase (Promega). Real-time quantitative PCR was performed using the Real-time PCR system 7300 (Applied Biosystems). In brief, the PCR amplification reaction mixtures (20 μL) contained cDNA, primer pairs, the dual-labeled fluorogenic probe, and Taq Man Universal PCR Master Mix (Applied Biosystems). The thermal cycle conditions included maintaining the reactions at 50°C for 2 min and at 95°C for 10 min, and then alternating for 40 cycles between 95°C for 15 s and 60°C for 1 min. The primer pairs and probe were obtained from Applied Biosystems. The relative gene expression for each sample was determined using the formula $2^{(-\delta\ Ct)} = 2^{(Ct\ (GAPDH)-Ct\ (target))}$, which reflected the target gene expression normalized to GAPDH levels.

Immunohistochemistry. Anti-EGFR, anti-HER2, anti-ERα, and anti-PgR were obtained from Ventana Medical Systems. Anti-CXCR4 was purchased from Prosci, Inc. Anti-MVP/LRP was obtained from Chemicon. Tissue sections were taken from 73 breast cancer patients who underwent radical surgery in the Department of Surgery, Kurume University Hospital, Japan, between 1993 and 1999. The 4-μm tissue sections were deparaffinized, and the slides were heated in a Cell Conditioning Solution buffer for 60 min at 100°C. The sections were stained using the BenchMark XT (IHC Automated System) and ChemMate ENVISION method (Dako Corporation). BenchMark XT was used for staining anti–YB-1, anti-ERα, anti-EGFR, anti-HER2, and anti-PgR. The ChemMate ENVISION method was used for immunochemical staining of anti-ERβ, anti–p-Akt, anti-CXCR4, and anti-MVP/LRP. The samples were viewed using an Olympus BX51 fluorescence microscope (Olympus). The extent of staining of YB-1, ERα, ERβ, and PgR proteins was classified based on the percentage of cells with strongly stained nuclei: ≥10% indicated that a gland was positive for YB-1, and ≤9% indicated that it was negative. EGFR and HER2 expressions were classified into four categories: score 0, no staining at all or membrane staining in <10% of tumor cells; score 1+, faint/barely perceptible partial membrane staining in >10% of tumor cells; score 2+, weak to moderate staining of the entire membrane in >10% of tumor cells; and score 3+, strong staining of the entire membrane in >10% of tumor cells. The extent of immunohistologic staining for EGFR was defined as follows: scores of 2+ or 3+ were regarded as positive, and scores of 0 or 1+ were regarded as negative. The extent of immunohistologic staining for HER2 was defined as follows: scores of 3+ were regarded as positive, and scores of 0 or 1+ or 2+ were regarded as negative. Immunohistochemical staining of p-Akt and CXCR4 was defined based on the percentage of cells with strong cytoplasmic staining as follows: ≥10% indicated that a gland was positive, whereas ≤9% indicated that it was negative. MVP/LRP staining was defined as follows: ≥50% of cells with a strongly stained cytoplasm indicated that a gland was positive, whereas ≤49% indicated that it was negative. All immunohistochemical studies were evaluated by two experienced observers who were blind to the conditions of the patients.

Statistical analysis. The associations between YB-1 and clinicopathologic findings (age, tumor size, menopausal status, histologic grade, and lymph node metastasis) and molecular markers were tested by Fisher's exact test, the χ^2 test, or the Wilcoxon rank-sum test, depending on the type of data. A P value of <0.05 was regarded as significant unless otherwise indicated. The relationships between YB-1 expression and overall survival/progression-free survival, as well as other clinicopathologic findings and molecular markers, were examined by the Kaplan-Meier method and the log-rank test. Hazard ratios (HR) were estimated by Cox regressions.

As YB-1 and the expression of receptors of the EGFR family and hormone receptors, as well as the clinicopathologic findings, were all correlated, we summarized them by means of their principal components and investigated the relationship between these components and overall survival/progression-free survival by Cox regression. The relationship between the principal components was found to be related to overall survival/progression-free survival, and the clinicopathologic findings and molecular markers were investigated by studying their correlations. In addition, to obtain a direct representation of the relationship between molecular markers, we used a graphical modeling technique incorporating logistic regressions; a path was drawn between two markers only if these markers were conditionally associated with a significance level of 0.1, given the other markers. The data on overall survival and progression-free survival in this analysis were updated on February 27, 2007.

Results

The knock-down of YB-1 alters the expression of EGFR, HER2, ERα, CXCR4, and MVP/LRP genes. We initially compared the expressions of YB-1 siRNA–treated and control MCF-7 breast cancer cells using a high-density oligonucleotide microarray. Of the 54,675 RNA transcripts and variants in the microarray, we identified differentially expressed genes containing 43 genes that were up-regulated >2-fold and 203 genes that were down-regulated 0.5-fold or less (Supplementary Table S1). It has been reported that the activity of PI3K/Akt was required for translocation of YB-1 into the nucleus (24, 27). We therefore investigated the effect of LY294002, a selective inhibitor of PI3K, in both T-47D and MDA-MB231 cells. LY294002 inhibited the

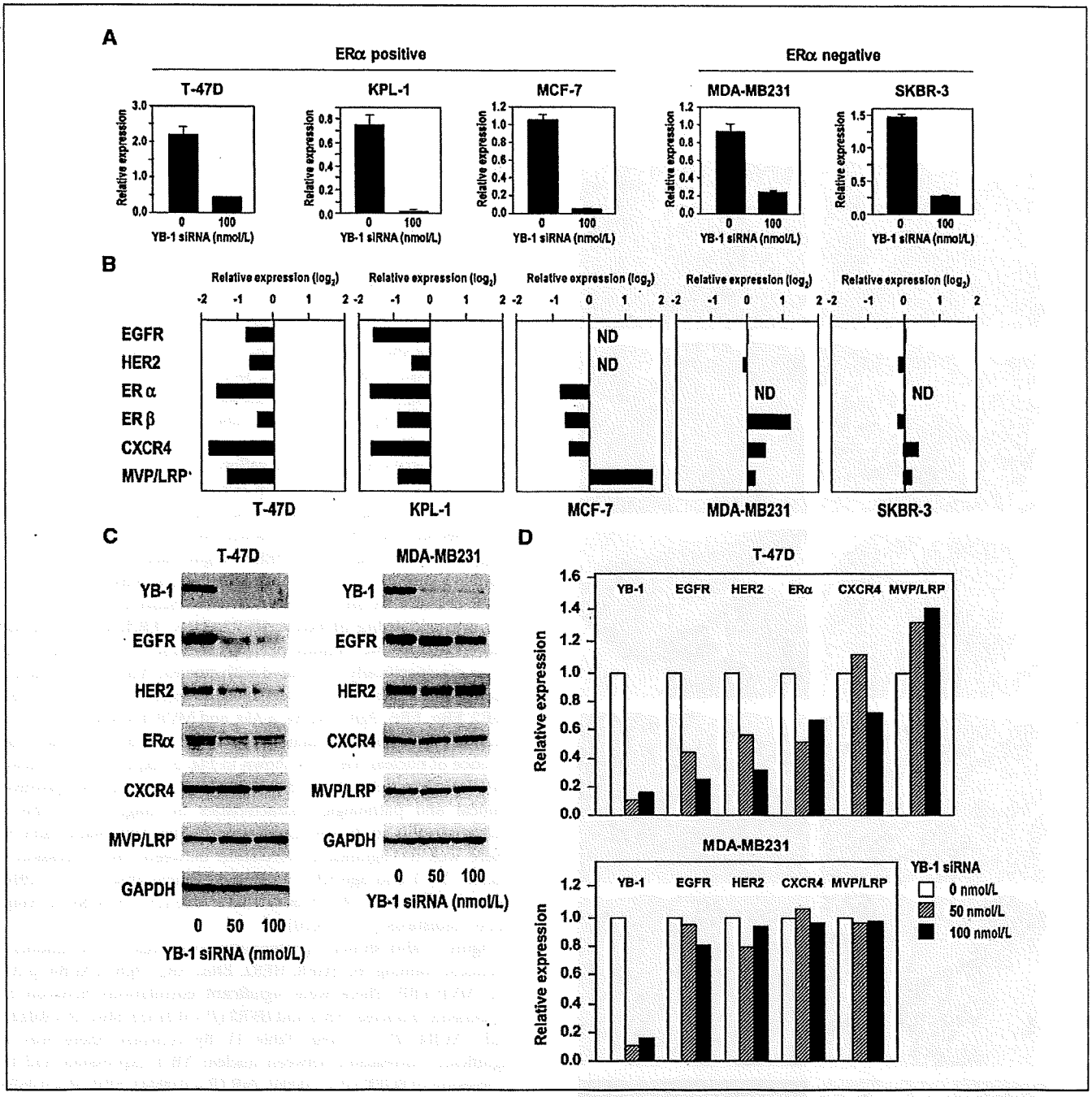

Figure 1. Effect of YB knock-down on expression of EGFR, HER2, ERα, CXCR4, and MVP/LRP in ERα-positive and ERα-negative breast cancer cells. *A*, YB-1 knock-down by treatment of YB-1 siRNA for 48 h. Relative mRNA expression was measured by qRT-PCR. *Columns*, mean of three independent experiments; *bars*, SD. *B*, levels of EGFR, HER2, ERα, ERβ, PgR, CXCR4, and MVP/LRP mRNA expression in YB-1 siRNA–treated cells. Changes of mRNA expression were expressed as the log of relative expression. *ND*, not detected. *C*, T-47D and MDA-MB231 cells were incubated with YB-1 siRNA for 72 h, and lysates were prepared. *D*, levels of YB-1, EGFR, HER2, ERα, CXCR4, and MVP/LRP expression were measured by densitometry.

nuclear expression of YB-1 in both cell lines (Supplementary Fig. S1*A*), consistent with previous reports (24, 27). We also examined whether PTEN status was correlated with nuclear YB-1 expression in breast cancer cells. Of the five human breast cancer cell lines used, cellular levels of the PTEN were not significantly correlated with nuclear expression levels of YB-1 protein (Supplementary Fig. S1*B* and *C*).

The differentially expressed genes included MVP/LRP and CXCR4, consistent with our previous study on human ovarian cancer cells (27). We next tested, by quantitative real-time PCR (qRT-PCR), whether the expression of CXCR4 and MVP/LRP was affected by knock-down of YB-1 in various human breast cancer cell lines. We also examined the expressions of growth factor receptors and hormone receptors, such as EGFR, HER2, ERα, and

ERβ, which are thought to be important target genes in breast cancer. The five cell lines used were as follows: T-47D, MCF-7, and KPL-1, which are ERα-positive; and MDA-MB231 and SKBR-3, which are ERα-negative. Transfection of YB-1 siRNA decreased the expression of YB-1 mRNA by ≥70% in all five cell lines (Fig. 1*A*). Both EGFR and HER2 mRNA levels were found to be decreased in YB-1 siRNA–treated T-47D and KPL-1 cells but not in MDA-MB231 and SKBR-3 cells (Fig. 1*B*). EGFR and HER2 mRNAs were not detected in MCF-7 cells. It has been reported that the 5′ regulatory region of the ERα gene contains several Y-box–like sequences. Cellular mRNA levels of ERα were reduced by YB-1 siRNA in T-47D, KPL-1, and MCF-7 cells by 74%, 75%, and 40%, respectively, (Fig. 1*B*). CXCR4 and MVP/LRP mRNA levels were also decreased in YB-1 siRNA–treated T-47D and KPL-1 cells but not in MDA-MB231 and SKBR-3 cells (Fig. 1*B*).

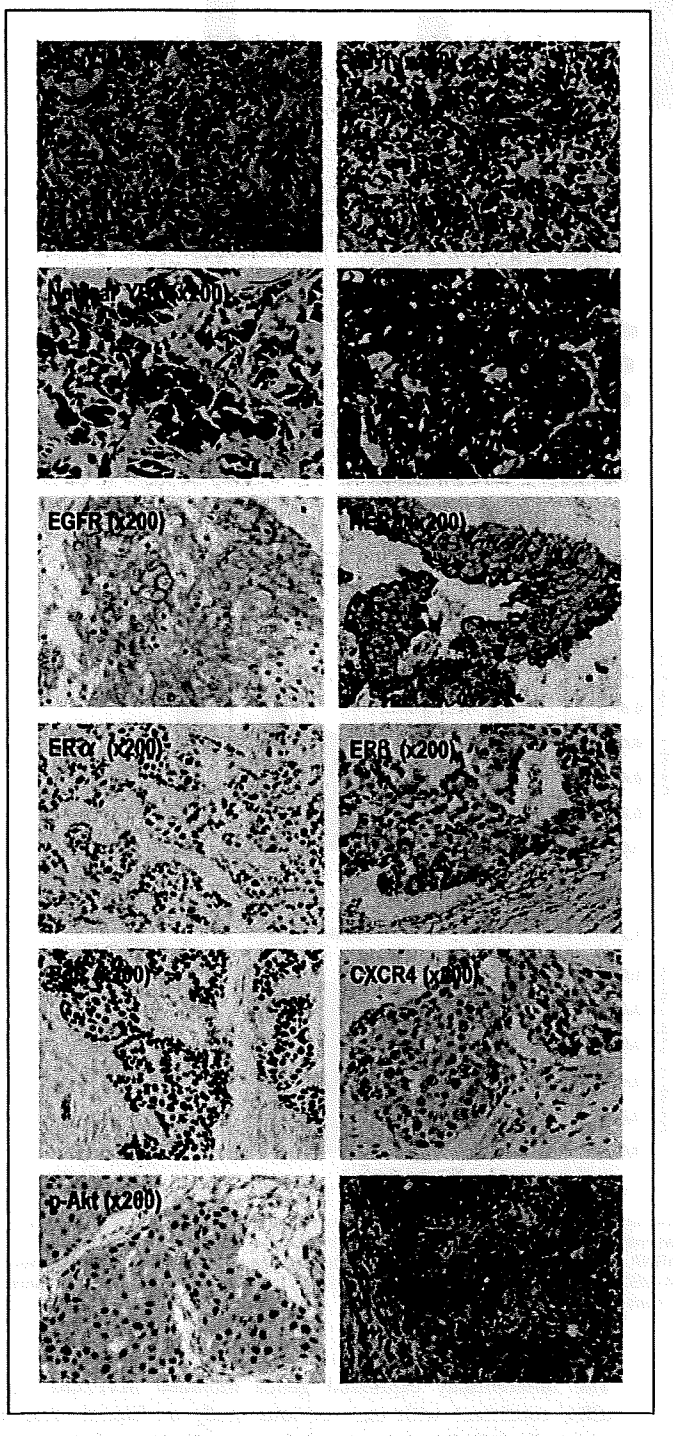

Figure 2. Histologic findings and expression of YB-1, EGFR, HER2, ERα, ERβ, PgR, CXCR4, p-Akt, and MVP/LRP in human breast cancer. YB-1 expression was recognized in two patterns: nuclear positive or negative. Cancer cells showed strong expression of EGFR and HER2 in the membrane. Strong expression of ERα, ERβ, and PgR was found in the nucleus. Moderate-to-strong expressions of CXCR4, p-Akt, and MVP/LRP were found in the cytoplasm.

Western blot analysis showed that siRNA to YB-1 decreased protein levels of EGFR, HER2, and ERα in T-47D cells; however, we did not observe decreased expression of EGFR and HER2 as a result of YB-1 knock-down in MDA-MB231 cells (Fig. 1*C* and *D*). These observations show that YB-1 only reduces the expression of EGFR and HER2 when ERα is present. Moreover, the expression of ERα was also affected by YB-1 knock-down. We next examined the causal relationship between HER2, ERα, and nuclear YB-1 in breast cancer cells in culture. Treatment with HER2-targeting trastuzumab blocked the nuclear localization of YB-1 in both T-47D and MDA-MB231, but the inhibitory effect was less in MDA-MB231 (Supplementary Fig. S2*A*). By contrast, nuclear YB-1 expression was not affected by ERα knock-down in T-47D cells in culture (Supplementary Fig. S2*B*). HER2 might directly modulate the cellular localization of YB-1 in breast cancer cells; however, ERα might not directly affect nuclear YB-1 localization.

Immunostaining of EGFR, HER2, ERα, ERβ, CXCR4, p-Akt, and MVP/LRP in human breast cancers. To examine which genes are specifically associated with nuclear YB-1 localization in human breast cancers, we selected eight molecular markers: EGFR, HER2, ERα, ERβ, PgR, CXCR4, p-Akt, and MVP/LRP. Representative immunohistochemical staining patterns in the presence and absence of nuclear YB-1 are shown in Fig. 2. Expression of nuclear YB-1 was detected in 30 of 73 patients (40%; nuclear YB-1 positive). Clinical and pathologic characteristics at diagnosis of the 73 patients in this study are summarized in Supplementary Table S2. There was no significant correlation between the expression of nuclear YB-1 and age ($P = 0.2562$), histologic grade ($P = 0.1910$), menopausal status ($P = 0.1508$), tumor size ($P = 0.1478$), or lymph node metastasis ($P = 0.0620$).

Figure 2 also shows representative examples of immunohistochemical staining for EGFR, HER2, ERα, ERβ, PgR, CXCR4, p-Akt, and MVP/LRP. There were significant correlations between the expression of nuclear YB-1 and HER2 ($P = 0.0153$), ERα ($P = 0.0122$), and CXCR4 ($P = 0.0166$; Table 1). By contrast, there was no significant correlation between nuclear YB-1 expression and the expression of EGFR ($P = 1.0000$), PgR ($P = 0.0944$), ERβ ($P = 0.0576$), p-Akt ($P = 0.0521$), or MVP/LRP ($P = 0.0577$).

Effects of nuclear YB-1 on survival and other molecular markers. The estimated product-limit survival functions of nuclear YB-1 are shown in Fig. 3*A* (overall survival) and Fig. 3*B* (progression-free survival), as well as the results of log-rank tests. Survival curves for patients with nuclear YB-1 were significantly different from those without nuclear expression ($P = 0.0139$ for overall survival; $P = 0.0280$ for progression-free survival). The results of log-rank tests for other factors are given in Table 2, showing that the tests for lymph node metastasis were significant ($P = 0.0001$ for overall survival; $P < 0.0001$ for progression-free survival).

The first eight principal components were used in the subsequent analysis, as their cumulative coefficients of variance

Table 1. Correlation between nuclear YB-1 expression and expression of eight target genes

Variables	All patients		Nuclear YB-1				*P*
			Negative		Positive		
	No. of patients	%	No. of patients	%	No. of patients	%	
EGFR							
Negative	58	79	34	79	24	80	1.0000
Positive	15	21	9	21	6	20	
HER2							
Negative	59	81	39	91	20	67	0.0153
Positive	14	19	4	9	10	33	
ERα							
Negative	24	33	9	21	15	50	0.0122
Positive	49	67	34	79	15	50	
ERβ							
Negative	18	25	7	16	11	37	0.0576
Positive	55	75	36	84	19	63	
PgR							
Negative	39	53	19	44	20	67	0.0944
Positive	34	47	24	56	10	33	
CXCR4							
Negative	29	40	12	28	17	57	0.0166
Positive	44	60	31	72	13	43	
p-Akt							
Negative	27	37	20	47	7	23	0.0521
Positive	46	63	23	53	23	77	
MVP/LRP							
Negative	41	56	20	47	21	70	0.0577
Positive	32	44	23	53	9	30	

were ~80%. Denoting the i-th principal component by PRINi, the results of Cox regression analysis were as follows. For overall survival, PRIN1 and PRIN7 were statistically significant [HR = 1.52 and $P = 0.0090$ (for PRIN1); HR = 2.06 and $P = 0.0499$ (for PRIN7); Fig. 4*A*]; and for progression-free survival, PRIN1, PRIN6, PRIN7, and PRIN8 were significant [HR = 1.59 and $P = 0.0009$ (for PRIN1); HR = 1.86 and $P = 0.0103$ (for PRIN6); HR = 2.30 and $P = 0.0078$ (for PRIN7); HR = 1.68 and $P = 0.0508$ (for PRIN8); data not shown]. PRIN1 was positively correlated with YB-1 [correlation coefficient (r) = 0.593], HER2 ($r = 0.397$), histologic grade ($r = 0.557$), tumor size ($r = 0.577$), and lymph node metastasis ($r = 0.522$). PRIN1 was negatively correlated with ERα ($r = -0.684$), PgR ($r = -0.453$), CXCR4 ($r = -0.460$), menopausal status ($r = -0.618$), and age ($r = -0.607$). This might indicate that some effect shared by YB-1, HER2, ERα, PgR, and CXCR4 leads to poor survival. PRIN7 was positively correlated with tumor size and negatively correlated with EGFR and p-Akt. Note that PRIN7 was not correlated with YB-1; this points to the existence of different mechanisms that influence survival apart from those involving PRIN1.

Stepwise variable selection was used to select the following molecular markers for graphical modeling: YB-1, HER2, ERα, ERβ, and CXCR4. Figure 4B shows the results of graphical modeling of these markers when two markers were positively correlated; a plus symbol is shown on the path, otherwise a minus symbol is shown. The relationships are indicated between markers; for example, YB-1 is related to CXCR4, ERβ, and HER2 but not directly to ERα. Note that HER2, YB-1, CXCR4, and ERα are correlated with PRIN1, emphasizing their important effects on survival.

Discussion

In this study, we assessed whether the expression of EGFR and ErbB2/HER2 was affected by YB-1 in breast cancers, as this might influence prognosis. We developed two independent approaches to identify which genes are under the control of YB-1 in human breast cancer cells. One approach involved microarray analysis, qRT-PCR, and immunoblotting to determine whether the expression of EGFRs, ERα, and other YB-1–related proteins is controlled by YB-1 in culture. The other approach consisted of immunohistochemical analysis of those protein molecules closely associated with nuclear localization of YB-1 in patients with breast cancer.

The expression of EGFR and HER2 was down-regulated by YB-1 knock-down in ERα-positive, but not ERα-negative, breast cancer cell lines, suggesting that YB-1 siRNA–induced suppression depends upon the presence of ERα. By contrast, immunohistochemical analysis showed that nuclear YB-1 expression was significantly associated with the expression of HER2 but not of EGFR. Janz et al. (6) have also reported a close association of YB-1 nuclear localization with the expression of HER2 in primary breast cancers. Moreover, Wu et al. (20) found that the introduction of a p-Akt–insensitive mutation into YB-1 markedly decreased the expressions of both EGFR and HER2, suggesting a close linkage between YB-1 and EGFR/HER2 expression in breast cancer cells in culture. YB-1 overexpression in human breast epithelial cells did not affect HER2 but caused up-regulation of EGFR, with concomitant EGF-independent phosphorylation of EGFR (18). The effect of YB-1 on EGFR and/or HER2 might depend in part on the particular cell line examined.

Oda et al. (11) found a highly significant association of p-Akt with nuclear YB-1 expression in human ovarian cancers, and both p-Akt and nuclear YB-1 expression were independent prognostic biomarkers; however, we observed no statistically significant association of p-Akt expression with nuclear YB-1 expression in our immunohistochemical analysis (Table 1). Cross-talk between growth factor receptors, such as EGFR, insulin-like growth factor (IGF) receptor, and estrogen signaling cascades occurs at the level of ERα (28, 29); this leads to activation of PI3K/Akt and ultimately to activation of ERα (30, 31). Thus, activation of ERα as well as YB-1 and its translocation to the nucleus seem to be coordinately controlled in breast cancer cells by the PI3K/Akt pathway in response to growth factors such as EGF/transforming growth factor α and IGF. PI3K/Akt activation could therefore be primarily dependent on the active state of ERα, which seems to play a major role in the nuclear translocation of activated YB-1 in ERα-positive breast cancer cells. In relation to a possible association of hormone receptors with nuclear YB-1 localization, we found that the

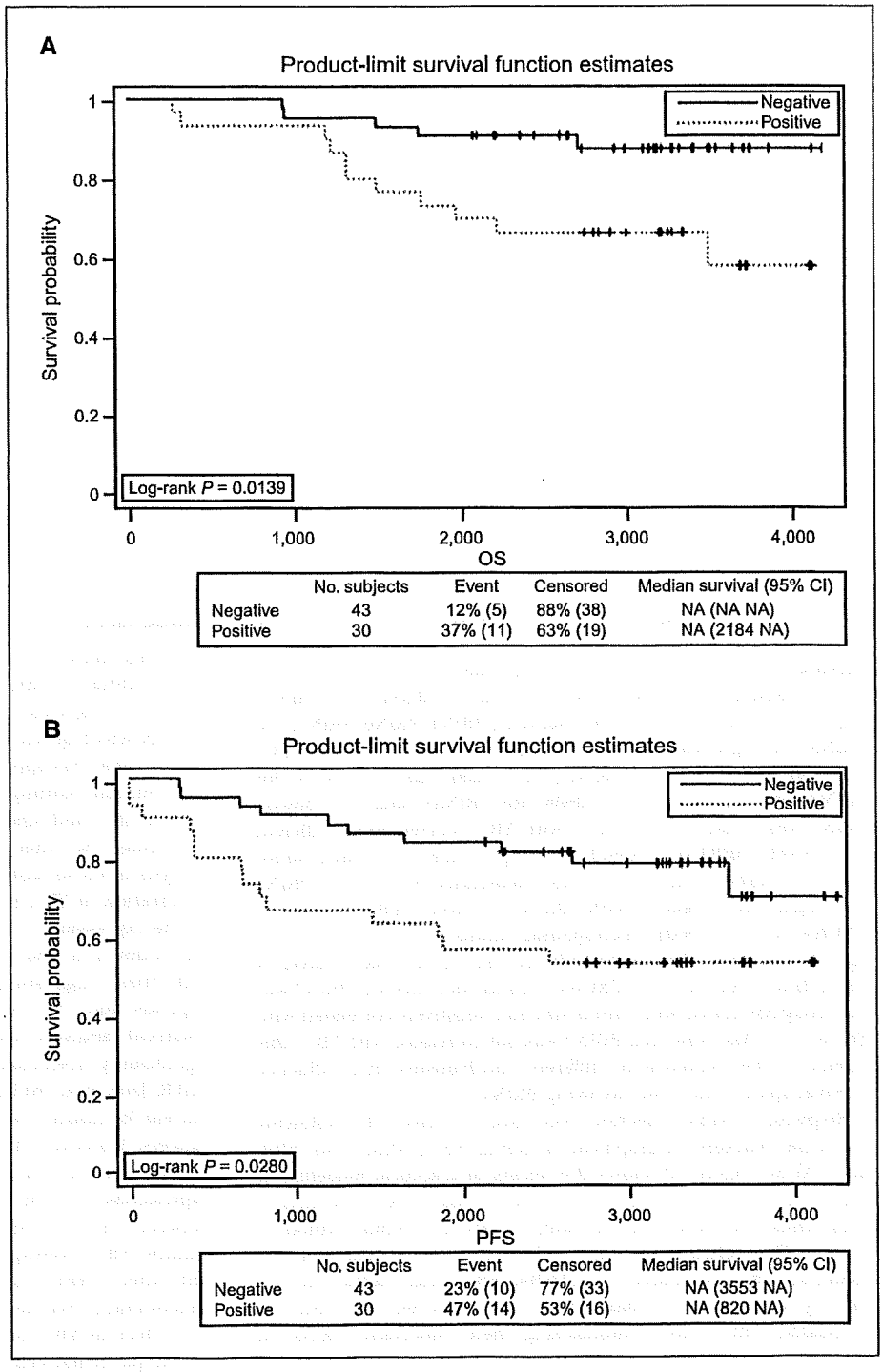

Figure 3. Kaplan-Meier overall survival (*A*) and progression-free survival (*B*) according to nuclear YB-1 expression in 73 patients with breast cancer. Nuclear expression of YB-1 has a significant predictive value for survival.